JOURNAL OF PETROLOGY

Journal of Petrology, 2020, Vol. 61, No. 10: egaa093
doi: 10.1093/petrology/egaa093
Advance Access Publication Date: 9 October 2020
Original Article

OXFORD

Fault-Controlled Magma Ascent Recorded in the Central Series of the Rum Layered Intrusion, NW Scotland

V. R. Troll [1,*], T. Mattsson[1,2], B. G. J. Upton[3], C. H. Emeleus[4,†], C. H. Donaldson[4,5], R. Meyer[6], F. Weis[1], B. Dahrén [1], and T. H. Heimdal[7]

[1]Department of Earth Sciences, Uppsala University, Villavägen 16, Uppsala SE-752 36, Sweden; [2]Department of Geological Sciences, Stockholm University, Svante Arrhenius väg 8, Stockholm 114 18, Sweden; [3]School of Geosciences, University of Edinburgh, West Mains Road, Edinburgh EH9 3JW, UK; [4]Department of Earth Sciences, Durham University, South Road, Durham DH1 3LE, UK; [5]School of Earth and Environmetal Sciences, University of St, Andrews, St, Andrews KY16 9AL, UK; [6]Service Géologique de Luxembourg, Ministère de la Mobilité et des Travaux Publics, 23, Rue du Chemin de Fer, Bertrange L-8057, Luxembourg; [7]CEED, University of Oslo, Sem Sælands vei 2A, ZEB-bygget, Oslo 0371, Norway

*Corresponding author. telephone: 0046-(0)18-471-2570; E-mail: valentin.troll@geo.uu.se
[†]Deceased.

Received 10 May 2019; Accepted 21 September 2020

ABSTRACT

The Palaeogene layered ultrabasic intrusion of the Isle of Rum forms the hearth of the Rum Igneous Centre in NW-Scotland. The regional Long Loch Fault, which is widely held to represent the feeder system to the layered magma reservoir, dissects the intrusion and is marked by extensive ultrabasic breccias of various types. Here we explore the connection between the layered ultrabasic cumulate rocks and breccias of central Rum that characterize the fault zone (the 'Central Series') and evaluate their relationship with the Long Loch Fault system. We show that fault splays in the Central Series define a transtensional graben above the Long Loch Fault into which portions of the layered units subsided and collapsed to form the extensive breccias of central Rum. The destabilization of the cumulate pile was aided by intrusion of Ca-rich ultrabasic magmas along the faults, fractures and existing bedding planes, creating a widespread network of veins and dykelets that provided a further means of disintegration and block detachment. Enrichment in LREE and compositional zoning in intra cumulate interstices suggest that the collapsed cumulates were infiltrated by relatively evolved plagioclase-rich melt, which led to extensive re-crystallization of interstices. Clinopyroxene compositions in Ca-rich gabbro and feldspathic peridotite veins suggest that the intruding magma was also relatively water-rich, and that pyroxene crystallized dominantly below the current level of exposure. We propose that the Long Loch Fault opened and closed repeatedly to furnish the Rum volcano with a pulsing magma conduit. When the conduit was shut, pressure built up in the underlying plumbing system, but was released during renewed fault movements to permit dense and often crystal-rich ultrabasic magmas to ascend rapidly from depth. These spread laterally on arrival in the shallow Rum magma reservoir, supplying repetitive recharges of crystal-rich magma to assemble the rhythmic layering of the Rum layered intrusion.

Key words: Rum Igneous Centre; Long Loch Fault; tectonic conduit opening; magma recharge

INTRODUCTION

A central theme in igneous petrology concerns the processes that modify magmas during magma storage, transport and differentiation. Key questions for petrologists relate to how magmas are fed into, and aggregate within, shallow crustal magma reservoirs and plutons

and how crustal plutons grow (laterally and vertically). Moreover, the relative roles of distinct magma chamber processes that drive magma diversification such as crystal settling vs *in situ* crystallization vs post-cumulus replacement reactions remain contentious (e.g. Brown, 1956; Donaldson, 1974, 1976; Irvine, 1980; Bédard *et al.*, 1988; Emeleus *et al.*, 1996; Irvine *et al.*, 1998; Holness, 2007; Marsh, 2013, 2015; Latypov, 2015; Leuthold *et al.*, 2015, 2014; Cashman *et al.*, 2017). This makes it desirable to learn more about the range of processes that operate in crustal magma reservoirs in order to improve our understanding of magma-storage and supply in ancient, as well as in active volcanic systems. In particular, the link between tectonic movements of the Earth's crust and magmatism has been discussed from several perspectives, but detailed application to individual volcanic systems is often not straightforward (e.g. van Wyk de Vries & Merle, 1998; Holohan *et al.*, 2008; Mathieu & van Wyk de Vries, 2011; Allan *et al.*, 2012; Cooper *et al.*, 2012; Upton, 2013; Hodgson & Young 2016; Trippanera *et al.*, 2018).

The Isle of Rum is an iconic site for igneous petrology as it hosts the famed layered ultrabasic Rum Layered Intrusion or Suite. The Layered Suite is widely known for the sixteen repetitive (rhythmic) macro units in the Eastern Layered Series that each grade upwards from peridotite to feldspar-rich gabbro or troctolite (Brown, 1956; Emeleus *et al.*, 1996; Emeleus, 1997; Emeleus & Troll, 2008, 2014). The Rum Layered Intrusion is divided into three major portions or 'Series', termed the Eastern Layered Series (ELS), the Western Layered Series (WLS), and the Central Series (CS), which make up the 'layered suite' (Fig. 1). Overall the layered ultrabasic Suite comprises ~60% peridotite, up to ~25% feldspar-rich gabbro (troctolite and allivalite) and ~15% of feldspathic peridotite and gabbro plugs. Igneous layering is common throughout the Rum Layered Suite and is developed right up to its margins, although intrusion breccias and later marginal gabbros frequently obscure the contact relationships (e.g. Greenwood *et al.*, 1990; Emeleus, 1997; Petronis *et al.*, 2009). The peridotites and troctolites of the Rum Layered Suite are usually layered on a centimetre to decimetre scale, which has been interpreted to imply a multitude of small to medium recharge and mixing events (e.g. Emeleus & Troll, 2014; Hepworth *et al.*, 2017). Overall lateral variations in peridotite vs troctolite within the Eastern Layered Series appear to reflect a more olivine-rich mineral assemblage toward the centre of the pluton (Emeleus *et al.*, 1996). This is in line with structural field data and magnetic fabric information that have been interpreted to indicate central downthrow or sagging towards the Long Loch Fault to accommodate the successive magma recharges (Volker, 1983; Volker & Upton, 1990; O'Driscoll *et al.*, 2007*b*). The N–S striking Long Loch Fault (LLF) traverses Rum and exposes a chaotic set of igneous breccias (the Central Series) that have previously been proposed to represent the formerly prime conduit for the Rum

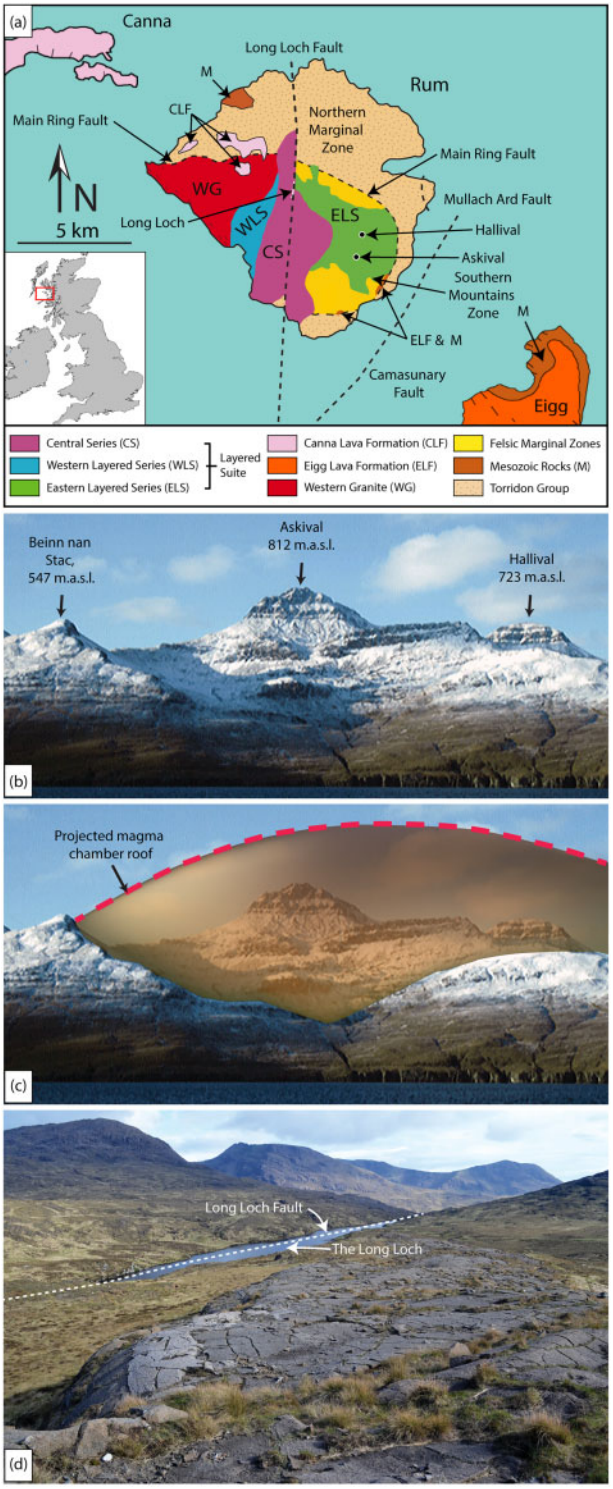

Fig. 1. (a) Geological map of the Isle of Rum. The Central Series is shown in purple and the Eastern and Western Layered Series in green and blue. The Palaeogene igneous centre is limited by the Main Ring Fault. The Long Loch Fault traverses the Rum Igneous Centre in a N–S direction and shows ~750 m post-magmatic offset. Modified after Emeleus & Troll (2008). (b) and (c) View of south-eastern Rum from offshore. The steeply inclined margin of the Layered Suite is exposed at Beinn nan Stac and allows an extrapolation of the former roof to the layered pluton. (d) View of Long Loch Fault zone in central Rum (viewed from north), marked by the Long Loch.

Igneous Centre as a whole (McClurg, 1982; Emeleus *et al.*, 1996; Emeleus, 1997; O'Driscoll *et al.*, 2007*b*; Emeleus & Troll, 2008, 2014; Petronis *et al.*, 2009; Fig. 1a and d). The detailed relationship of these breccias with the Long Loch fault and the rhythmically layered Eastern and Western Series is, however, not yet fully resolved (Emeleus *et al.*, 1996; Emeleus and Troll, 2014) and forms the main target of the current work.

The abundant and diverse ultrabasic breccias of the Central Series have been discussed for well over 50 years (Wadsworth, 1961, 1992; Donaldson, 1975; McClurg, 1982; Volker, 1983; Emeleus *et al.*, 1996). While most workers agree that the Central Series is linked to the Long Loch Fault, two mechanisms of breccia formation have been proposed (1) the Central Series was created by wholesale subsidence of layered ultrabasic units during movement along an active Long Loch fault (e.g. Wadsworth, 1961, 1992), or alternatively, (2) breccias were created by intrusion of new material along the active Long Loch Fault, thereby separating the Western and Eastern Layered Series and brecciating the existing layered suite along the divide (e.g. Donaldson, 1975; McClurg, 1982; Volker & Upton, 1990). The second concept would have involved pulses of intrusive uplift followed by partial collapse once the intrusive pressure subsided.

In this paper, we offer an interpretation of the relationship between the Long Loch Fault and the Central Series in order to explain the emplacement processes of the Rum Igneous Complex and in particular that of the Rum Layered Series. We seek to demonstrate that regional tectonics, via the Long Loch Fault, have played a crucial role in the siting of the Rum magma chamber system and, we argue, also in modulating magma influx into the active magma reservoir at the time of formation. To do so we provide new field data, structural observations and models, petrographic observations, whole-rock and trace-element compositional data, mineral data, estimates of crystallization pressures, and magmatic H_2O contents combined with available information to develop an overall model for the formation of the Rum Igneous Centre.

METHODS

Structural analysis and 3D modelling

In order to discern the major structural features, attitudes of layering, fault orientations, and lithological variations were recorded in the field. To better visualize the recorded geological structures, the structural data collected during our work and that of Emeleus (1997) were processed in 3 D with the Midland Valley/Petex Ltd software package *MOVE*^{TM} (www.mve.com). Structural features were projected onto a DEM (Digital Elevation Model) of Rum's topography (OS sheet NM39, 10 m accuracy, OS OpenData is free to use under the Open Government Licence, OGL) and extrapolated as down-dip planes for 500 m The structural features recorded in the field were also integrated with information from satellite imagery (source: *Esri, DigitalGlobe*) and the satellite images were processed in *Esri ArcGIS*® by manual drawing of polylines onto observed lineaments. The lineaments were then imported into *MOVE*^{TM}, where the 'Line to Strike' conversion tool was used to provide a large set of structural information. Several of the peridotite and gabbro plugs are reported as more or less vertical sheet intrusions or pipes (Holness, 1999; Holness *et al.*, 2012), which allowed for analyses of their shape-preferred orientation (SPO). The shapes of vertical to sub-vertical plugs on the Rum map (Emeleus, 2004) were drawn manually as polygons in *Esri ArcGIS*®, then imported into the open source image analysis software *ImageJ* (Schneider *et al.*, 2012), and converted into a binary image. Plug shapes were analysed with *ImageJ* and their preferred orientation obtained with the software *CSDcorrections* version *1.55* (Higgins, 2000; Higgins, 2002). Horizontal gabbro and peridotite sheets were excluded from the SPO analysis.

Electron probe micro analysis

Representative samples of the Central Series rocks were collected and include feldspathic peridotite (dykes and veins), gabbro veins and the 'pebbly' peridotite, to complement previously published petrographic observations and geochemical data. The collected samples were used to prepare polished thin sections, which were analysed using the field emission electron probe micro-analyser (FEG-EPMA) JXA-8530F JEOL HYPERPROBE at Uppsala University. The instrument was used in Electron Dispersive Spectroscopy (EDS) mode to identify mineral phases and in Wavelength Dispersive Spectroscopy (WDS) mode for quantitative geochemical analysis of individual mineral grains. The electron beam was set to 15·0 kV and 10 nA for olivine and pyroxene, with a diameter of 2 μm. A beam diameter of 5 μm was employed for plagioclase. The FEG-microprobe is equipped with five spectrometers for WDS analysis using different crystals. Spectrometers one and two used TAP crystals to analyse Na, Al and Si, Mg. Spectrometers three and four used PETJ crystals to analyse Ca, Mn, K, Ba and Ti. Spectrometer five utilized a LIFH crystal to analyse Fe, Va, Ni and Cr. The built-in PRZ correction was implemented during all measurements. The Na and Ca distribution in interstitial plagioclase of three samples was analysed using 800×800 μm WDS element maps. For the maps the electron beam was set to 15·0 kV and 4 nA with 100 ms dwell time and the composition was analysed every μm in the map area. The following calibration and standards were used during analysis: pyrophanite for Mn and Ti, magnesium oxide for Mg, albite for Na, orthoclase for K, baryte for Ba, aluminium oxide for Al, fayalite for Fe, nickel oxide for Ni, chromium oxide for Cr, and wollastonite for Ca and Si. Uncertainties: SiO_2, Al_2O_3, MgO and CaO $\leq$ 1·5% s.d., FeO $\leq$ 2·2% s.d., Na_2O in plagioclase and clinopyroxene $\leq$ 4·5% s.d., and minor elements $\leq$ 10% s.d. (see Barker *et al.*, 2015). All major

element mineral data collected during this study are provided in Supplementary Table 1; supplementary data are available for downloading at http://www.petrology.oxfordjournals.org.

Fourier transform infrared spectroscopy (FTIR)

To estimate the water content of a magma, the H_2O-content in nominally anhydrous clinopyroxene can be used (e.g. Nazzareni *et al.*, 2011; Okumura, 2011; Weis *et al.*, 2015). Infrared (IR) spectra identify OH-vibrational bands in the minerals, and together with compositional data from microprobe analysis, the partition coefficient between H_2O and the magma can be established. These data were then employed to obtain an estimate of the water content of the magma from which the mineral (e.g. pyroxene) crystallized (O'Leary *et al.*, 2010; Nazzareni *et al.*, 2011; Weis *et al.*, 2015).

Seven large clinopyroxene crystals from three gabbro vein samples were prepared for analysis as described in Weis *et al.* (2015). The water content was analysed using both sample compartment of an Equinox 55 spectrometer as well as a Bruker Hyperion 2000 microscope equipped with a NIR source (halogen lamp), a CaF_2 beam-splitter, a wire-grid polarizer (KRS-5) and an InSb detector at the Natural History Museum, Stockholm. For each crystal a polarized IR spectrum over the range 2000 to 5000 cm^{-1} was measured along the directions of the main refractive indices (α, β and γ) to obtain the total absorbance: $A_\alpha+A_\beta+A_\gamma=A_{total}$. A_α and A_γ were measured on the (010) crystal face and A_β on (100). Crystal thickness varied between 110 and 900 μm for both the (100) and (010) faces. Cracks and inclusions in the crystals were avoided by using small apertures (100 to 400 μm) for masking during the analysis. For each individual spectrum, 128 scans were performed and subsequently averaged. No significant differences between the analyses in the sample compartment and microscope measurements were observed. The individual IR spectra were viewed in the Peakfit® software and were baseline corrected. By using the integrated area under the corrected OH-bands, the corresponding water contents were calculated.

To derive the water content of the magma from which the analysed pyroxenes crystallized, the EMPA data of the pyroxenes and the equation by O'Leary *et al.* (2010) ($\ln D = -4{\cdot}2(\pm0{\cdot}2) + 6(\pm0{\cdot}5)^{VI}[Al^{3+}]-1(\pm0{\cdot}2)[Ca^{2+}]$) were used to determine mineral/melt partition coefficient for water between clinopyroxene and its host magma. The overall error for the magmatic water contents is similar to the IR-analysis (±20%) (Libowitzky & Rossman, 1997; Weis *et al.*, 2015) (Table 1).

XRF and ICP-MS analyses

Whole-rock samples were powdered in an agate ball mill and analysed with X-ray fluorescence spectroscopy (XRF) at the University of Bergen, Norway, on a Phillips PW1404 instrument. High Resolution Inductively Coupled Plasma Mass Spectrometry (HR-ICP-MS) was employed for trace element analysis using a Thermo Scientific Element2 HR-ICP-MS instrument. Sample powder aliquots of 100 mg were dissolved for ICP-MS analyses in acid (4 mL sub-boiled 22 M HF and 3 mL 14 M HNO_3) in PTFE screw-top beakers. The samples were completely digested after 48 h at a temperature of 120 °C. 1 mL monitor solution with 10 ppm Re, 5 ppm In and 2·5 ppm Tl was added to the sample solution, and dried to evaporate HF and extract Si as SiF4. Residues were dissolved again in 5 mL 14 M HNO_3 acid at 130 °C. For the ICP-MS measurements 1 mL solution was then diluted with ultrapure 18.2 MΩ water to 50 mL 2% HNO_3. Calibration curves using geological reference materials were produced with data from the Geological and Environmental Reference Materials (GeoReM) database (www.georem.mpch-mainz.gwdg.de). Good linearity was attained for most analytes, e.g. $R^2>0{\cdot}998$ for rare earth elements (REE) and high field-strength elements (HFSE). Standards BIR-1 and AGV-2 were used to monitor analytical accuracy; deviations from the standards values were generally <5%. For full details on sample preparation and data calibration see Meyer & van Wijk (2015).

THE RUM IGNEOUS CENTRE

Geological setting

During the early Palaeogene several large volcanoes formed in the present-day NW-British Isles. These, together with associated basalt lava fields and dyke swarms, constitute the British and Irish Palaeogene Igneous Province (BIPIP) (Bell & Williamson, 2002; Emeleus & Bell, 2005; Preston, 2009). The province includes the well-known igneous centres, Ardnamurchan, Mull, Rum, Skye, Slieve Gullion and the Mourne Mountains, whose study gave rise to some fundamental concepts in igneous petrology and volcanology, such as cone sheets, ring-dykes and cauldron subsidence and magma types (Bailey *et al.*, 1924; Richey, 1961; Le Bas, 1971; Emeleus & Bell, 2005). Many of the BIPIP volcanic complexes had an initial felsic volcanic phase, but subsequent intrusions generally shifted towards extensive mafic magmatism (Walker, 1975; Gamble, 1979; Kerr *et al.*, 1999; Troll *et al.*, 2000, 2004; Meade *et al.*, 2014).

The main tectonic features relevant to the BIPIP include several NE–SW-trending terranes that are separated by large bounding faults (e.g. Emeleus & Bell, 2005; Hopper *et al.*, 2014; Horni *et al.*, 2017). Rum is situated in the northernmost Hebridean terrane, whose major lithological units are Mesozoic strata and Neoproterozoic Torridonian sandstone overlying Archaean and Palaeoproterozoic Lewisian gneiss basement (e.g. Park *et al.*, 2002; Emeleus & Bell, 2005). Palaeogene tectonic stresses in the BIPIP left a set of NNE–SSW and NW–SE-trending strike-slip faults associated with a N–S regional compression, in addition to swarms of NW–SE-trending regional dykes that reflect an earlier NE–SW extensional regime (Jolly &

Table 1: FTIR analyses of Central Series gabbro vein clinopyroxenes and calculated magmatic water contents

Sample	$[H_2O]_{cpx}$ (ppm)	Si^{4+}	$^{(IV)}Al^{3+}$	Ca^{2+}	$lnD_{(cpx\text{-}melt)}$	$D_{(cpx\text{-}melt)}$	$[H_2O]_{Melt}$ (wt. %)	Error 1σ (wt. %)
C-Gabbro1 (crystal 1)	295	1·87	0·126	0·86	−4·237	0·014	2·04	±0·41
C-Gabbro1 (crystal 2)	426	1·87	0·126	0·86	−4·237	0·014	2·95	±0·59
C-Gabbro2-A (crystal 2)	382	1·893	0·107	0·86	−4·360	0·013	2·99	±0·60
C-Gabbro2-B (crystal 1)	378	1·895	0·105	0·85	−4·367	0·013	2·98	±0·60
C-Gabbro2-B (crystal 3)	306	1·895	0·105	0·85	−4·367	0·013	2·41	±0·48
Per-Har-Vein (crystal 1)	409	1·89	0·113	0·86	−4·322	0·013	3·08	±0·62
Per-Har-Vein (crystal 2)	445	1·89	0·113	0·86	−4·322	0·013	3·35	±0·67

C-Gabbro2: B crystals are larger than A crystals.

Sanderson, 1995; Macdonald *et al.*, 2009, 2015; Cooper *et al.*, 2012; Hopper *et al.*, 2014). Palaeogene tectonics were probably controlled by interaction of pre-existing structures with those formed during: (1) Atlantic rifting, (2) the arrival of the Iceland plume, and (3) far-field hinterland tectonics (England, 1988; Lawver & Muller, 1994; Meyer *et al.*, 2007; Cooper *et al.*, 2012; Horni *et al.*, 2017).

The Rum Igneous Centre, dated at 60·53 ± 0·08 (U–Pb) Ma (Hamilton *et al.*, 1998), appears to be the earliest of all the central-type, sub-volcanic complexes of the Hebrides. Although picritic magmas played some part in other centres (e.g. Skye and Mull) the Rum Central Complex is singular in that such magmas apparently played a dominant role and reached near-surface levels over (inferentially) many thousands of years (Emeleus, 1997; Upton *et al.*, 2002; Emeleus & Troll, 2014).

The Rum Igneous Centre grew on a horst that separated two Mesozoic basins of the Hebridean Terrane (Emeleus, 1997). Magma upwelling at Rum initially produced a silicic collapse caldera with associated eruptions of rhyodacite ash-flows and emplacement of shallow-level micro-granites (Emeleus, 1997; Troll *et al.*, 2000; Donaldson *et al.*, 2001; Petronis *et al.*, 2009). The silicic magmas were generated by partial melting of country rocks during ascent of mafic magma (Troll *et al.*, 2004; Meyer *et al.*, 2009; Nicoll *et al.*, 2009), and these early silicic events are commonly summarized as Stage 1. Stage 2, focuses on the layered ultrabasic pluton that commenced with intrusion of basaltic dykes and cone-sheets, followed by emplacement of the main ultrabasic Layered Suite (Emeleus *et al.*, 1996; Emeleus & Troll, 2008, 2014) (**Fig. 1**). In addition, emplacement of the Layered Suite caused deformation of the Western Granite (WG) where anisotropy of magnetic susceptibility and palaeomagnetic measurements indicate that the microgranite has been tilted by ∼14° to the northwest (Petronis *et al.*, 2009).

The shallow emplacement level of the Rum Igneous Complex is indicated by the 'plutonic' cumulate sequences lying next to the Stage 1 extrusive rhyodacites (Emeleus, 1997; Holness, 1999; Holness & Isherwood, 2003; Troll *et al.*, 2008). Indeed, a volcanic superstructure had long been postulated (e.g. Brown, 1956). This is because the layered units are dominantly composed of olivine and calcic plagioclase crystallized from basaltic magmas, even though pyroxene, sodic plagioclase, magnetite etc. would have been significant components of such magmas. The scarcity of lower temperature residual fractions from the layers led Brown (1956) to postulate the growth of a basaltic volcano above the layered units. Vigorous erosion soon set in after magmatism ceased (Emeleus, 1997; Chambers *et al.*, 2005; Troll *et al.*, 2008). Evidence for fast erosion is found in NW Rum where the Western Granite and sandstones of the Torridon Group are overlain by basaltic lavas of the Canna Lava Formation (≤59 Ma) and their intercalated fluviatile conglomerates that contain clasts (cobbles) derived from contemporaneous erosion of the Rum pluton (e.g. Emeleus, 1985, 1997; Emeleus & Troll, 2008). Erosion was probably aided by displacement along local fault systems, like the Camasunary fault (Fig. 1a.), which had a history of activity starting already in the Mesozoic, and the Long Loch Fault, on which ≥750 m of post-magmatic lateral offset is recorded (Emeleus, 1997) (Fig. 1a and d), and may indicate dissection of the volcano during its growth. The geology of the Isle of Rum thus records the remarkable history of a fault-centred Palaeocene volcanic system from initial updoming and anatexis to its closing stages dominated by erosion and decay (Emeleus, 1997; Emeleus & Troll, 2011, 2014).

The layered ultrabasic pluton

The external boundaries of the Eastern, and part of the Western Layered Series are controlled by the Main Ring Fault (Brown, 1956; Emeleus *et al.*, 1996), which defines an ovoid ∼8 km E–W by ∼4 km N–S in map view. A pronounced positive Bouguer gravity anomaly over Rum was initially interpreted as indicating a steep-sided, approximately cylindrical body, of dense ultrabasic rock extending to a depth of ∼16 kilometres (McQuillin & Tuson, 1963; Emeleus *et al.*, 1996). Alternatively, if a tabular or disc-shaped body with a narrower feeder is assumed (mushroom-geometry) to explain the gravity anomaly, a higher proportion of dense peridotite would be required at depth than what is presently exposed in outcrops (Emeleus *et al.*, 1996; Emeleus, 1997). Albeit representing slightly different stratigraphic levels that are now separated by the Central Series, the Eastern and Western Layered Series are widely regarded as lateral equivalents of a formerly continuous cumulate pile that formed in a shallow crustal magma chamber, (Wadsworth, 1961, 1992; Donaldson, 1975; Emeleus

et al., 1996; Emeleus, 1997). The long axis of the Central Series coincides with the N–S Long Loch Fault (Fig. 2), which extends beyond Rum southwards to at least the nearby Camasunary fault and is part of the wider tectonic framework of the region (c.f. England, 1988; Smith, 2012). It continued to undergo right-lateral movement after magmatism on Rum had ceased (Emeleus, 1997). These fault movements along the Long Loch Fault during the Palaeogene probably played a crucial role in injection and replenishment of magmas into shallow crustal reservoirs (Donaldson, 1975; Emeleus, 1997; O'Driscoll *et al.*, 2007*b*; Petronis *et al.*, 2009; Emeleus & Troll, 2014).

The Eastern Layered Series is formed by a prominent succession of sixteen mostly gently-dipping layers of mafic and ultrabasic rocks that amount to ~750 m of total thickness (Brown, 1956; Emeleus, 1997). The ultrabasic portions consists of peridotite that grades upward into olivine-plagioclase troctolites (the so-called allivalite of Harker, 1908; Brown, 1956; Wager & Brown, 1968), or into anorthosite or gabbroic cumulates. 'Allivalite' (named after Hallival mountain) is a local term describing a dominantly olivine-plagioclase rock with >50 modal % plagioclase that is $\geq An_{80}$ (c.f. Harker, 1908; Brown, 1956), but we follow Bédard *et al.* (1988) and the IUGS nomenclature and we now employ the more familiar term troctolite in this account. Moreover, we refer to olivine–plagioclase rocks as feldspathic peridotites and to olivine-dominated rocks as peridotite. Successive layers of troctolite and feldspathic peridotite or peridotite may be separated by thin (millimetre scale) chrome–spinel seams (locally refered to as 'chromitite'). Traditionally the layered units are envisaged as having crystallized from discrete pulses of basaltic magma that precipitated chrome–spinel first, followed by olivine and then plagioclase to progressively form a typical 'unit', but more recent work suggests that stratiform Cr-spinel seams may have formed from reactive lateral melt migration that may have exploited lateral boundaries between successive cumulate units (c.f. Brown, 1956; O'Driscoll *et al.*, 2009, 2010; Leuthold *et al.*, 2015; Hepworth *et al.*, 2020*b*). Moreover, the layered units of the ELS tend to become more feldspathic (i.e. with decreasing thickness ratio of peridotite: troctolite) as traced eastwards away from the supposed Central Series feeder zone (see Fig. 5 of Volker & Upton, 1990). Although the processes by which one of the typical layered units (peridotite with overlying troctolite) remain conjectural, Volker & Upton (1990) suggest that the olivine-laden magmas deposited a high proportion of their crystal load close to the feeder zone.

The Western Layered Series is ~500 m thick and is composed of feldspathic peridotite that is at least in part underlain by layered gabbro (Wadsworth, 1961, 1992; Emeleus, 1997). Large-scale layering is less obvious in the Western Layered Series compared with the Eastern Layered Series, but small-scale layering marked by crystal laminations and variations in size and abundances of olivine and plagioclase is frequently present. Importantly, rocks of the upper Western Layered Series are virtually indistinguishable in the field from the Eastern Layered Series west of Barkeval (Fig. 2; Emeleus *et al.*, 1996). Notably, a remarkable type of crescumulate was first described from the Western Layered Series and called 'harrisite' (Harker, 1908; Wager *et al.*, 1960). It occurs in both peridotite and olivine gabbro layers, and is composed of dendritic olivine crystals up to 1 m in length (Harker, 1908; Wadsworth, 1961; Wager & Brown, 1968; Donaldson, 1974, 1976). The harrisitic textures of the Western Layered Series probably grew in short-lived periods of tranquillity from crystal-poor, high-Mg magma and crystal growth times were short, perhaps on the order of days or even less (Wager *et al.*, 1960; Wadsworth, 1961; Donaldson, 1982; O'Driscoll *et al.*, 2007*a*). The distinctive skeletal olivines that define harrisites are attributed to rapid crystallization from supersaturated high-Mg magma (Fig. 3). Once crystallization commenced, growth on the existing substrate was dominant, forming complex 'crystal gardens' on the magma chamber floor (Donaldson, 1974, 1976; O'Driscoll *et al.*, 2007*a*). In addition, platy harrisitic olivines present in layered peridotites on the southern slopes and east of Ard Nev probably broke off from the harrisite crystal gardens during times of increased turbulence or convective motion in the reservoir and are locally arranged in imbricate geometry (Emeleus *et al.*, 1996; O'Driscoll *et al.*, 2007*a*; Emeleus & Troll, 2008, 2014). This provides a sense of flow direction of the magma and mushes in this part of the Central Series, recording dominantly an inward flow, i.e. toward the centre of the pluton (O'Driscoll *et al.*, 2007*b*). There have also been observations of harrisite in intrusive sheets and veins in both the Eastern Layered Series and the Central Series (e.g. Donaldson, 1982; Hepworth *et al.*, 2017, 2020*b*).

The layered rocks of Rum have traditionally been interpreted in terms of magmatic sedimentation within a larger crustal magma reservoir and are regarded as classic magma chamber floor cumulates (e.g. Brown, 1956; Emeleus *et al.*, 1996; Emeleus, 1997). Layering is widely demonstrated by mineral lamination, modal mineralogy and grain size. Structures that indicate slumping and load deformation, as well as cross-bedding, are common, e.g. in Units 13 and 14 of the Eastern Layered Series, and a multitude of small but dynamic events is thus recorded in the Layered Suite (Holness *et al.*, 2012; Emeleus & Troll, 2014; Hepworth *et al.*, 2017, 2020*b*).

Several sheet-like intrusions of gabbros and feldspathic peridotite occur within the layered rocks. For instance, the bytownite gabbro ('eucrite') of Unit 9 has been shown to be a later intrusion (Bédard *et al.*, 1988; Holness *et al.*, 2007). In addition, a number of plugs as well as crystal-rich picrite dykes intrude the Rum Layered Suite (e.g. Upton *et al.*, 2002; Holness *et al.*, 2012), which underline the importance of frequent small-volume recharge events. Moreover, evidence for reactive liquid flow (c.f. Irvine, 1980; Holness 2007), i.e.

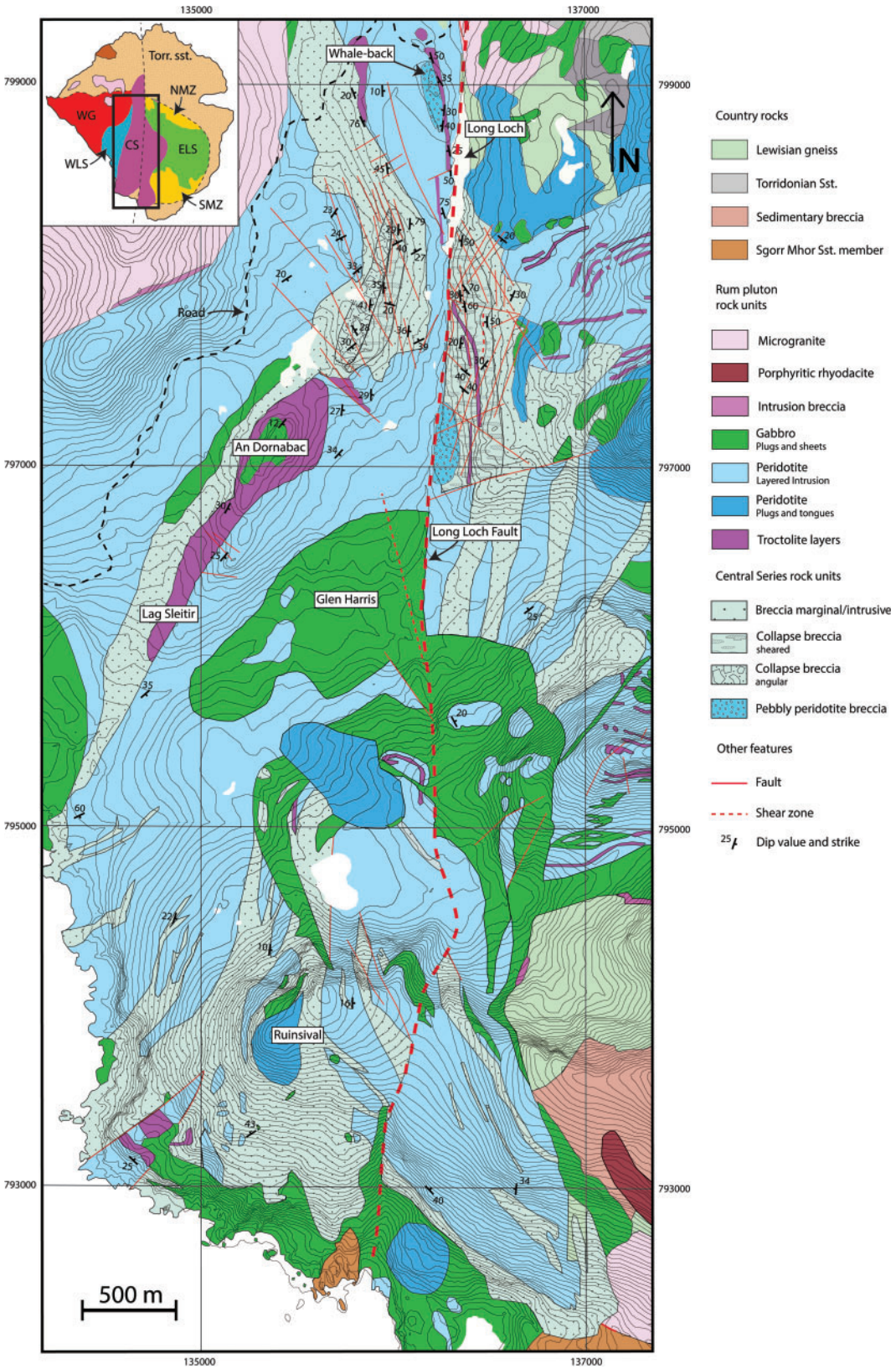

Fig. 2. Geological map of the Central Series based on mapping of the Central Series by McClurg (1982), Volker (1983) and Emeleus (1997), and modified after Emeleus (2004) with added information on distinction of breccia types, and minor faults (Mattsson, 2014). Note that the intrusive breccia is located on the marginal zones of the Central Series, whereas closer towards the central Long Loch Fault collapse breccias are more common. Moreover, outcrops of 'pebbly' peridotite are found exclusively along the trace of the Long Loch Fault.

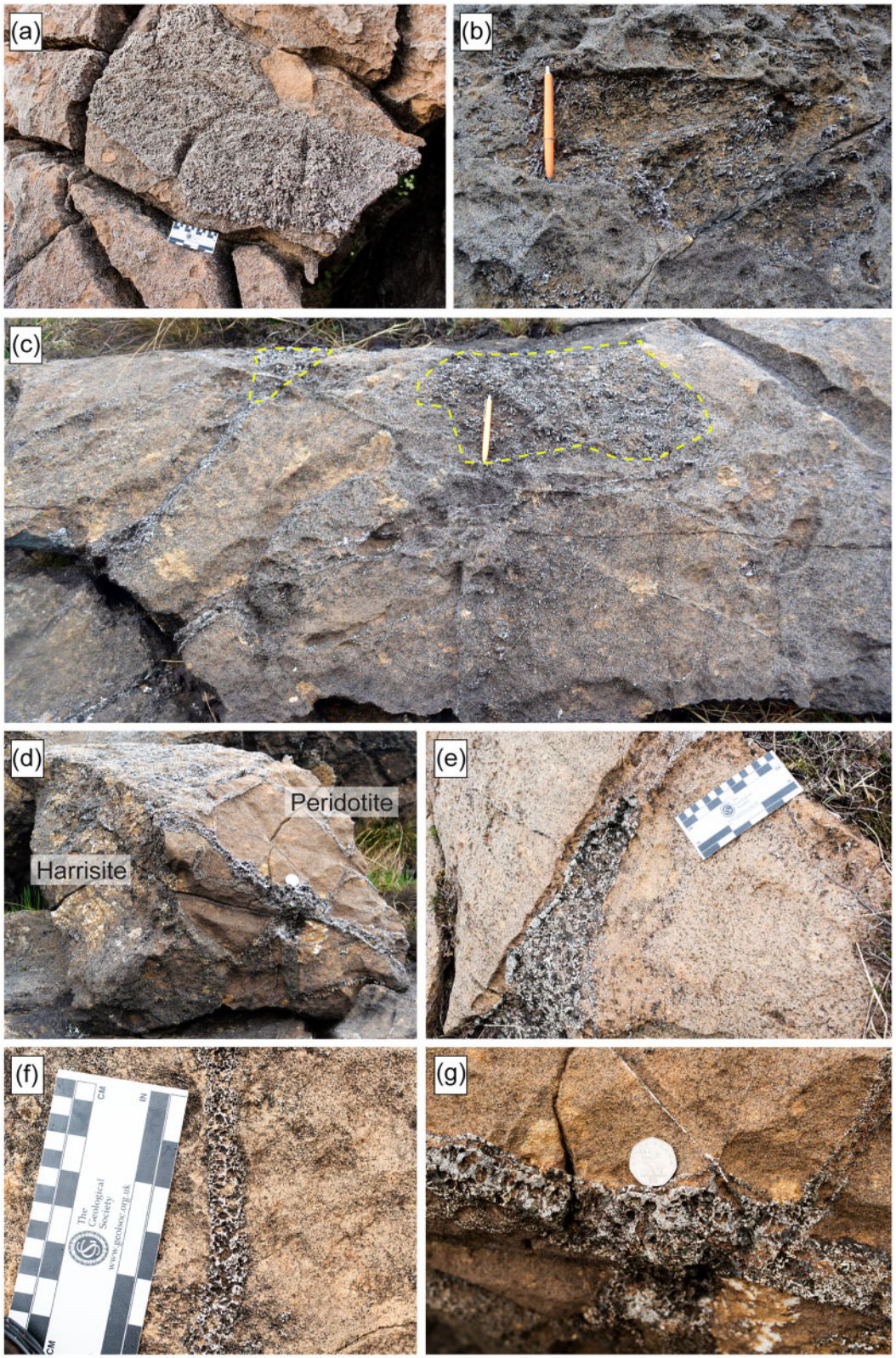

Fig. 3. Varieties of harrisite and feldspathic peridotite in the Central Series of the Rum Layered Suite. (a) Block with well-developed harrisite in feldspathic peridotite in the breccias of the An Dornabac ridge. (b) Branching harrisite olivine in the Central Series. (c) and (d) Feldspathic peridotite (grey) that infiltrated massive peridotite (brown) after deposition in the Long Loch Fault zone. Note that the feldspathic peridotite displays harrisite textures. Pen for scale in **(c)** and coin in (d**)**. The breccia blocks and clasts here originate from the Eastern and Western Layered Series. (e) Infiltrating gabbro vein cutting peridotite. Gabbro vein shows abundant dark pyroxene crystals (dark spots).(f) and (g) Close-up of feldspathic peridotite veins and offshoots cutting peridotite. The larger hollows in the vein in **(**g) reflectpicked out grains of olivines and pyroxenes. Coin for scale.

movement of high-temperature interstitial melts and fluids in the cumulate pile and reaction with crystals, is widespread. This process locally caused considerable modification of the original textures, crystal compositions, and rock compositions (e.g. Butcher, 1985; Bédard *et al.*, 1988; Holness 2007; Holness *et al.*, 2007; O'Driscoll *et al.*, 2010; Leuthold *et al.*, 2014, 2015; Hepworth *et al.*, 2020*a*, 2020*b*).

The Central Series

The intensely brecciated Central Series, first defined by McClurg (1982), is separated from the Eastern and Western Layered Series along steep brecciated marginal zones that are usually only a few hundred metres wide. At its northern end, the Central Series covers a tract of relatively low ground (Fig. 1d), reflecting its greater susceptibility to glacial erosion, probably as a result of the faulted and comparatively weaker and often altered nature of its rocks (Emeleus 1996). The igneous breccias of the Central Series contain blocks and clasts of olivine-rich peridotites, feldspathic peridotites and troctolite of up to house-size (Figs 4 and 5) (Wadsworth, 1961, 1992; McClurg, 1982; Volker & Upton, 1990; Emeleus *et al.*, 1996). The breccias are highly heterogeneous with respect to the relative abundances of matrix and clasts and range in texture from matrix-supported to clast-supported (e.g. Wadsworth, 1961; Donaldson, 1975; Volker & Upton, 1990). Breccia blocks also vary in shape from angular to partly rounded and some breccia clasts have been deformed into lenticular or sigmoidal shapes, while others appear to have been rigid as recorded by soft-sediment deformation (Figs 4–6) (Brown, 1956; Wadsworth, 1961; Emeleus, 1997). Accordingly, some clasts and blocks were derived by brittle fracturing and collapse of lithified roof and wall lithologies to the Central Series, while others represent contorted crystal-mushes that were still ductile on final emplacement (Figs 4–6; Donaldson, 1975; McClurg, 1982; Wadsworth, 1992; Emeleus *et al.*, 1996; Emeleus, 1997; Emeleus & Troll, 2008, 2014). Although many of the clasts in the Central Series were mechanically coherent, cumulus material has also locally migrated down-slope as viscous parcels or tongues of mushy material (**Fig. 6**), implying that reworking/mobilization of unconsolidated crystal mushes occurred in addition to brittle disintegration of already solidified cumulate units. In the central portion of the Central Series, a rock made of well-sorted centimetre-sized rounded to angular pebbles of peridotite in feldspathic peridotite crops out in elongate outcrops and transport and size-sorting of clasts appears to have played a role in its formation (see also below).

The dip of layering in individual blocks in the Central Series breccias ranges from steep to shallow and although uniform within blocks, it appears random on outcrop scale. Individual blocks or clasts often record complex events (e.g. intermittent crystal accumulation, *in situ* crystal growth and subsequent replacement reactions), while layered structures in the enclosing peridotite matrix usually record disturbance due to subsidence of blocks into ductile crystal mushes (e.g. Fig. 6a and b). Throughout the Central Series, troctolites are also strongly deformed with common folding, evidence of fault drag and boudinage structures (Volker, 1983). An overall assessment by Wadsworth (1992) led him to suggest that generation of the breccias was accompanied by repeated subsidence events.

Major intrusive components in the Central Series, besides the plugs (see below), are the abundant millimetre to decimetre thick veins and dykelets of feldspathic peridotite and gabbro. These are extremely widespread in the Central Series and range from concordant with layering to transgressive with respect to layering. They locally reach an abundance that can be viewed as 'pervasive infiltration' (Fig. 3d), suggesting incipient brecciation that likely also promoted rock-disintegration within the Central Series. The lack of chilled contacts to the veins implies that the Central Series rocks were still hot when intrusion of the veins and dykelets took place (c.f. Marsh, 1981). The intrusive feldspathic peridotite veins, dykes and pods commonly show harrisitic textures in the Central Series (Fig. 3), which contrasts with the primarily layer-bound occurrence of harrisite in the Western and Eastern Layered Series (e.g. O'Driscoll *et al.*, 2007*a*; Hepworth *et al.*, 2017, 2020*b*). Breccia matrix compositions are variable and range from pyroxene-rich (up to 40% modal) to olivine-rich (up to 30% modal); but feldspathic peridotite is predominant, with 40–50% plagioclase (Donaldson, 1975; Volker & Upton, 1990). Wadsworth (1992) identified the matrix rocks as poorly compacted cumulates (i.e. meso-cumulates) with a significant percentage of intercumulus material. There are numerous internal intrusive contacts among the breccias and shearing is commonly present close to the marginal breccias, where vertical fabrics have been imposed on dunitic peridotite wall-rocks up to 20 m away from the margins of the Central Series (Volker, 1983).

In an attempt to place the observations in a stratigraphical context, Wadsworth (1961) and later McClurg (1982) and (Volker, 1983) divided the Central Series into four stratigraphic sub-units (compare Fig. 2). (1) The Outer Breccia (or Lag Sleitir Breccia), (2) the An Dornabac member, (3) the Long Loch member, and (4) the Ruinsival stratigraphic members. While an element of *in-situ* stratigraphy is possible, we argue that these observed stratigraphic units in the Central Series probably reflect inherited successions linked to the Eastern and Western Layered Series that broke apart during activity along the Long Loch Fault and may therefore contain layered segments that are no longer preserved in either the Eastern or the Western layered intrusions (Volker & Upton, 1990). Arguments against an *in situ* stratigraphy in the Central Series, include: (1) the larger and steeply inclined masses of layered troctolite south of the Long Loch that closely resemble troctolite in the higher units in the Eastern Layered Series (McClurg,

Fig. 4. Breccia types of the Central Series: (a) Collapse breccia with jumbled metre-sized blocks of layered peridotite and troctolite fragments; SE of the Long Loch. (b) Broken up intrusion breccia from the western margin of the Central Series with pervasive network of thin feldspathic peridotite veins and dykelets (grey) that infiltrated the host peridotite (brown), west of Lag Sleitir ridge. (c) Matrix-supported feldspathic peridotite breccia. Fragments of dunitic peridotite (brown to yellow) were seemingly deposited into a feldspathic peridotite magma or mush near the boundary with the Eastern Layered Series. Note pen for scale in image centre.

Fig. 5. (a) Stratigraphy of the An Dornabac ridge (compare Fig. 2). The bottom unit is an intensely sheared breccia, while at the top unit is a collapse breccia with angular troctolite clasts. In-between these two units, several seemingly coherent peridotite and troctolite layers dip towards the Long Loch Fault. Sitting person for scale (circled). (b) Close-up of the lower sheared breccias. (c) Zoomed in photograph of troctolite breccia clasts in the sheared unit. The clasts are generally oriented parallel to the overall direction of movement. This lower sheared breccia probably formed when larger slabs (mega-blocks) of layered peridotite and troctolite slid on a 'décollement' towards the Long Loch Fault. (d)–(e) Details of the upper angular troctolite breccia show a brown peridotite matrix that contains metre-sized internally layered-clasts. This breccia-type probably formed by deposition of smaller debris blocks and clasts on the large raft-like mega-blocks that slid into the peridotite mush of the Central Series. Sitting person in **d** and standing person in (**e**) for scale.

1982); Emeleus et al., 1996; Emeleus, 1997); (2) the An Dornabac Member of the Central Series shows striking similarities with the Ard Mheall Member of the Western Layered Series (Wadsworth, 1992); (3) faulted walls that leave steep-sided escarpments on the margins of the Central Series (Emeleus, 1997); (4) slump-structures are common at certain horizons in the Eastern Layered Series (e.g. units 7 and 14, Brown, 1956; Emeleus *et al.*, 1996; Emeleus, 1997) and in combination with common flat-lying overfolds in the Eastern Layered Series troctolites, and with the thin, attenuated and wispy feldspathic peridotite layers, evidence for transport of material towards the intrusion centre is widely indicated (c.f. Volker, 1983; Renner & Palacz, 1987; Emeleus & Troll, 2014). This inference is consistent with the magmatic fabric interpretation in the Eastern Layered Series and that of the Western Granite (O'Driscoll *et al.*, 2007*b*; Petronis *et al.*, 2009) and also with the major disruption of incompletely-consolidated cumulates in the Eastern Layered Series observed on Trollaval's westernmost

slopes (Volker & Upton, 1990). There, units high in the cumulate succession reveal increasingly steep westward dips (up to 80°), which culminate in broke-off troctolite layers that appear to have collapsed into the Central Series (Volker & Upton, 1990); (5) Finally, the comparable eastward flexure towards the Central Series present in the Western Layered Series (e.g. north of Loch an Dornabac). This flexure displays layer dips that increase to >40° towards the Central Series and grades into a zone of large angular mega-blocks in the adjacent portion of the Central Series that are derived from several lithological units (McClurg, 1982; Wadsworth, 1992; Mattsson, 2014). Intrusion by upwelling crystal-rich mafic magmas, now represented by veins and dykelets, probably acted as lubricant and aided disintegration of formerly coherent cumulates (Donaldson, 1974).

A number of remarkable petrographic features exist in the Central Series. These include olivines that are frequently dark brown to black due to a multitude of small (5–10 micron) opaque inclusions or lamellae. Slow annealing in a system that experienced persistent cooling and re-heating has been shown to be a possible cause for this phenomenon (c.f. Haggerty & Baker, 1967; D'Oriano *et al.*, 2013; Ejima *et al.*, 2015), consistent with repeated magma recharge into the Central Series. Another notable feature is the 'poikilo-macro-spherulitic feldspar' textures from, for example, the Dornabac area of the Central Series, that were originally interpreted to represent the result of the emplacement of a batch of magma consisting of olivine crystals with 'basalt' melt in between (i.e. a slurry), from which the melt solidified in the spaces between the olivines. However, the nucleation rate of new plagioclases was very low, making for a restricted number of nuclei, thus promoting the branching of growing interstitial crystals (Donaldson *et al.*, 1973). The examples from An Dornabac comprise massive radial and braid-like growths of calcic, often bytownitic plagioclase that is poikilitically enclosing olivines. Like the harrisite olivines, these textures are now recognised in many places over the Central Series and beyond. Notably, however, some workers have described an association with intruded feldspathic peridotite veins and dykelets (Volker, 1983; Mattsson, 2014) (Fig. 7e and f). Despite olivine composing ~60% of the rocks in the Central Series, the poikilitic feldspars radiate outwards in semi-symmetrical patterns, and up to diameters of ~1 m. The crystals are typically linked as twins and form meshes of planar stellate structures that range from patchy to radiating (Donaldson *et al.*, 1973). At several sites in the Central Series, crystal gardens of 'poikilo-macro-spherulitic feldspar' textures have seemingly grown from a substrate upward (Fig. 7). The radiating and branching nature of the plagioclase crystals seen here on Rum remains enigmatic. The possibility exists that some of these textures may also reflect local recrystallization due to, for example, fluids and heat that percolated upwards through the cumulate pile to crystallize poikilo-macro spherulites.

There are about 40 peridotite, gabbro and/or dolerite plugs on Rum and traditionally they have been divided into those penetrating the Layered Series and those outside the pluton (Emeleus, 1997). In map-view, specific plugs tend to vary in shape from circular to elongate in N–S direction, and there are three end-member types that can be distinguished: (1) Plugs with simple circular plan that suggest simple cylindrical conduit plugs, (2) elongate (i.e. syntectonic) plugs and tongues parallel to faults, and (3) mushroom-style gabbro intrusions (Fig. 8). Of the olivine–gabbro plugs and sheets intruding the Central Series (Fig. 2), the largest is the semi-circular Glen Harris gabbro, which demonstrates that basaltic magmas occurred throughout the evolution of the Rum Layered Suite (c.f. Nicoll *et al.*, 2009). The Glen Harris gabbro plug also records post-solidification offset along the Long Loch Fault of ~750 m (Fig. 2). The Papadil plug has a peridotite core surrounded by a gabbro shell (c.f. Holness *et al.*, 2012), whilst the Ruinsival plug is dominated by feldspathic peridotite. The Barkeval plug is heterogeneous and is generally poorly-layered peridotite with an approximately 80 m wide marginal zone of heterogeneous feldspathic peridotite near Barkeval summit (Volker & Upton, 1990). Whereas the peridotitic and gabbroic plugs cutting the ultramafic complex lack discernible thermal aureoles, those in the north cutting the Torridonian sandstones, generated marked thermal aureoles (Holness, 1999; Holness *et al.*, 2012). The outcrops of the northern plugs present cross-sections of near-vertical conduits through which ultramafic magmas flowed for periods of up to several months, presumably supplying surface eruptions (Holness, 1999; Holness *et al.*, 2012). Some of these plugs are themselves cumulates, reflecting terminal consolidation conditions following cessation of magma supply (Holness *et al.*, 2012).

Structural relationships between the Central Series and the Long Loch Fault

Fault splays and lenses in connection to the Long Loch Fault are common in the Central Series, as are faults within breccia blocks and breccia mélanges (Figs 4, 5, 6 and 9). Many fault splays are expressed as straight furrows (up to several metres wide) or as terraces between outcrops (Fig. 9) and are considered to signify displacement and dilation, as well as intrusion by feldspathic peridotite (now removed by erosion). Notably, steeply dipping feldspathic peridotite veins are commonly parallel to fault splays, while shallowly dipping veins frequently reflect layering-parallel veins and dykelets in clasts and blocks of the Central Series. However, significant dilation appears to be lacking in some late faults that visibly displace troctolite units. The traces of the dilated faults grade in some instances into shear zones intruded by feldspathic peridotite and these show frequent shear indicators, such as sigmoidal shaped clasts (Fig. 9c and d). The fault splays generally dip steeply towards the Long Loch Fault and have numerous

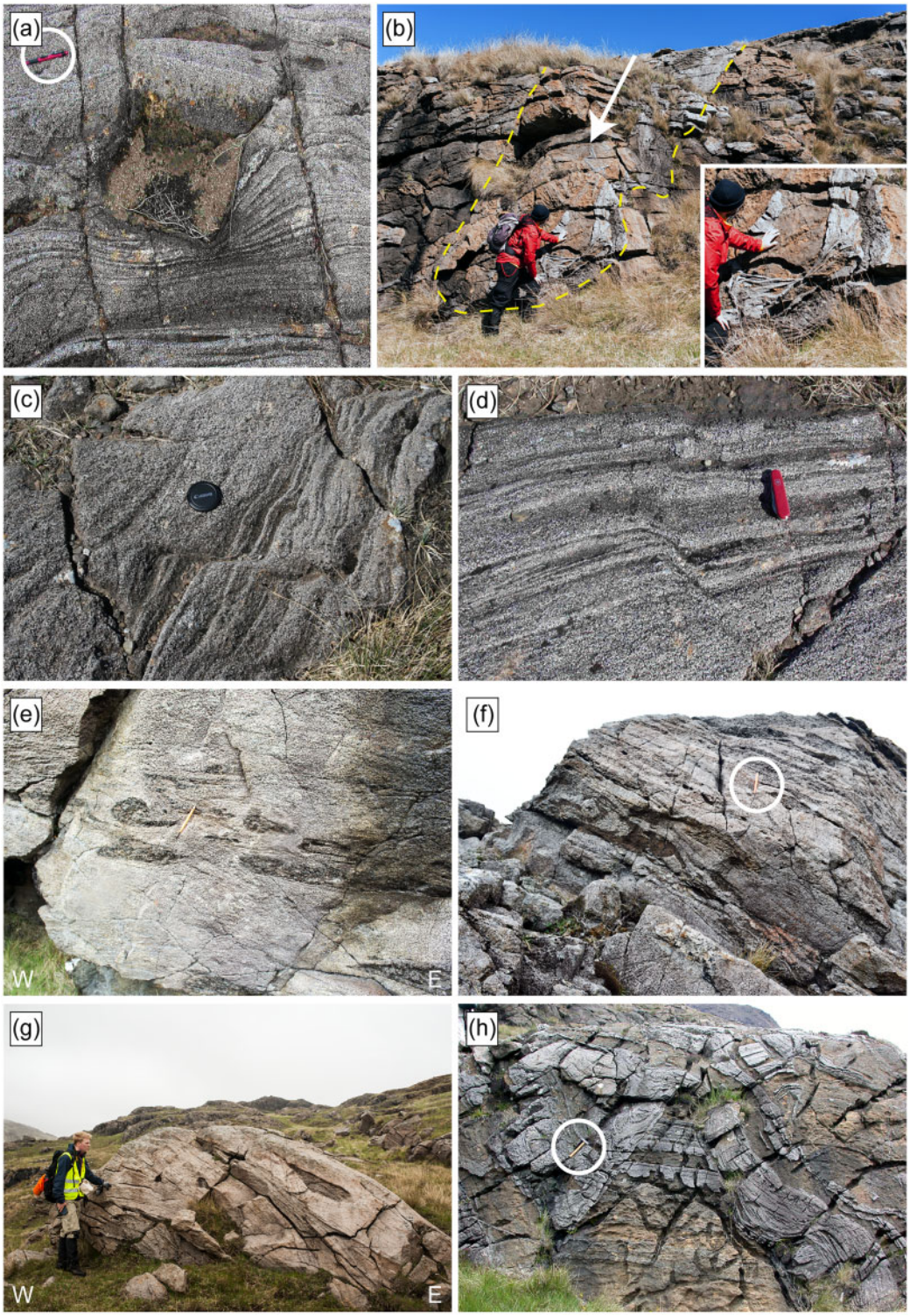

Fig. 6. (a) Example of formerly rigid dropstone in layered troctolite, Central Series, north of the 'whale-back' (see text for details). In close proximity are folds and faults of layered rocks interpreted as products of slumping of accumulated crystal mushes. The ductile normal faults were probably caused by rapid down-throw towards the Long Loch Fault. (b) Formerly ductile slab of layered peridotite (brown) and troctolite (grey) that was draped over a peridotite breccia surface visible to the left and right, near NE shore of Long Loch. Inset shows a close-up of the once ductile peridotite and troctolite slab that flowed over an existing clast-rich breccia deposit as a ductile mush.(c)–(d) Minor normal and partly annealed fault in layered cumulates north of the Long Loch. The layers, now essentially vertical, are inferred to have originally been quasi-horizontal. Camera lens cap and pocket-knife for scale. (e) Sheared gabbroic clasts that form lenses and schlieren in host olivine troctolite at Lag Sleitir. Orange pen for scale. (f) and (g) Outcrop views of troctolite (light grey rock) with flattened and partly folded feldspathic peridotite inclusions (darker schlieren), Lag Sleitir. Pen and person for scale, respectively. (h) Rugged former 'chamber floor topography' overlain by formerly ductile slumps and rafts of troctolite, NE shore of Long Loch. Hammer for scale.

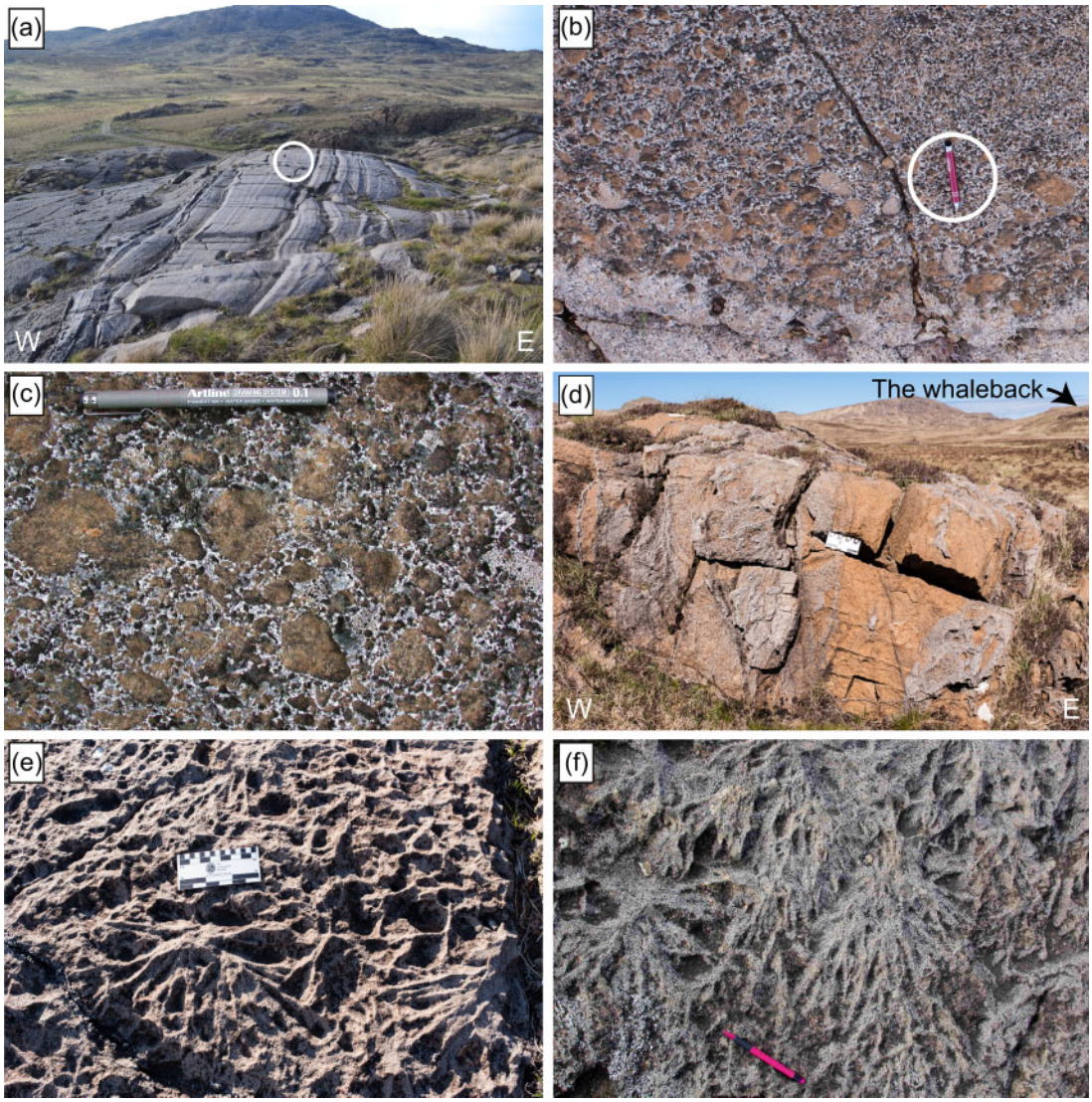

Fig. 7. (a) The northern 'whale-back' outcrop shows W-dipping troctolite (light grey) and 'pebbly' peridotite layers (dark grey, to the left). Encircled walking stick is ~1 m in length. (b) Graded 'pebbly' peridotite (brownish grey) in contact with troctolite (light grey) at the 'whale-back' outcrop. Pen for scale. (c) Close-up of the 'pebbly' peridotite in (b). The peridotite clasts are rounded and were preferentially deposited in topographical lows and thus most probably formed from currents within the magma chamber. Pen for scale. (d) The continuation of the troctolite layering, ~1 km south of the whale-back outcrop. Layers dip steeply and record ductile slumping and intense intrusion veining by feldspathic peridotite. Scale card in centre is 15 cm across. (e) Examples of Poikilo-macro-spherulite plagioclase texture in the Central Series, Pervasive poikilo-macro-spherulites near Loch an Dornabac, and (f) SE of the Long Loch. Extensive poikilo-macro-spherulitic structures are widespread but may occur in association with intrusive feldspathic peridotite veins, representing either nucleation and growth at distinct centres (c.f. Donaldson *et al.*, 1973) and/or may be especially prolific near intrusive dyklets and veins. Some of the poikilo-macro-spherulites verge preferably in one direction. Pen for scale.

intersections that create fault-bounded slivers and lenses (Figs 9 and 10), defining a concentrically grading ('onion skin style') graben geometry in map view that shows progressively bigger fault lenses away from the central fault zone (Fig. 10). Blocks within these fault lenses frequently record highly variable dips between blocks, indicating that raft-like 'mega-blocks' or slabs have collapsed into the Long Loch Fault graben in an oblique to normal fashion (sliding), and a rotational movement can be demonstrated for several medium to large blocks in the field (e.g. Figs 4 and 5). Furthermore, steeply inward-dipping rock faces on the western side of the Long Loch valley suggest a steep overall dip of the Long Loch Fault towards the west (Emeleus, 1997). Fault splays in the western Central Series are dominantly NW-striking, and, moreover, a shear zone in the Glen Harris gabbro in the southern Central Series strikes parallel to several fault splays in the western Central Series. Persistence of faulting during Central Series evolution is emphasized by the observation that faulting in the Ruinsival area pre-dated intrusion of late-stage gabbro (Volker, 1983). The trend of most major structures in the Central Series is broadly N–S, consistent with the orientation of the Long Loch Fault. In addition,

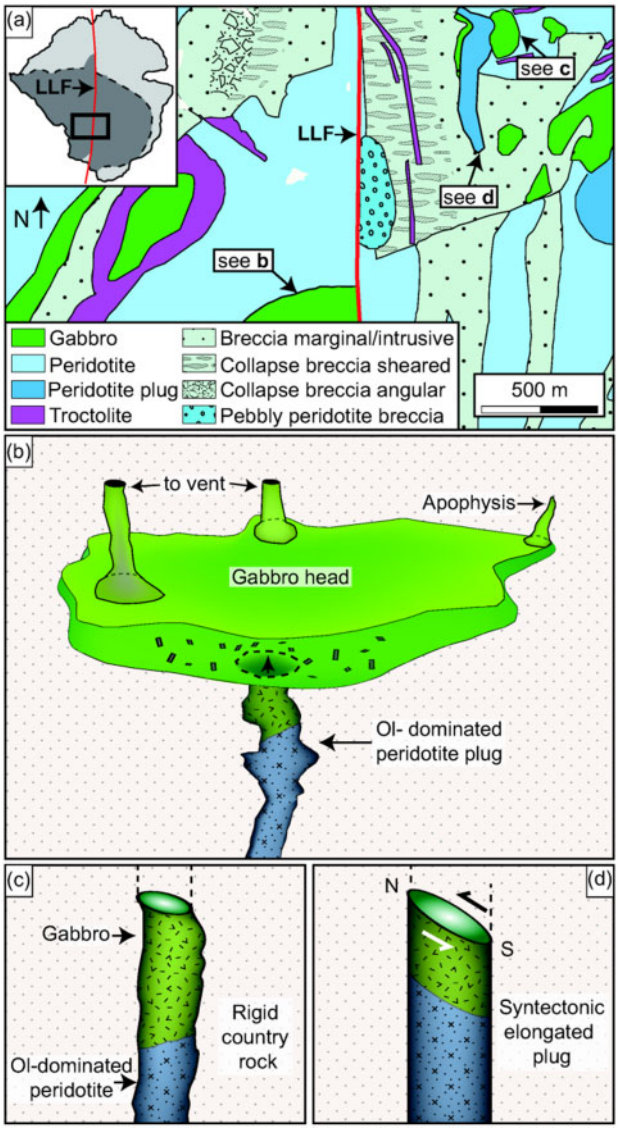

Fig. 8. (a) Sketch map of the central part of Central Series, emphasising the three types of plugs found in the Central Series. Schematic cross-sections of (b) mushroom- or umbrella-like gabbro intrusion that probably connected to feeder plugs below and above. (c) Simple semi-circular conduit plugs of gabbro or peridotite that show no tectonic influence, reflecting intrusion during periods of tectonic quiescence. (d) Syntectonic plugs, with notable N–S elongations, which probably intruded during periods of active deformation along the Long Loch Fault (see text for details).

tectonic lineaments (assumed to represent faults) in the Central Series are clearly traceable in satellite imagery and can be divided on the basis of different trends (1) NW–SE, (2) NNE–SSW, and (3) NE–SW into three groups (Fig. 10a and b). A dominantly NW–SE trend is, in turn, inferred from peridotite and gabbro plugs in the Torridonian sandstone north of the Central Series that also appear to be fault-controlled (Fig. 11). East and south of An Dornabac, a large slab composed of layered peridotite and troctolite (Fig. 5a), dips ~30° to the ESE and is cut by frequent fault splays and by veins of feldspathic peridotite. In the northwestern breccia zone, structures are more chaotic with steep and shallow layering recorded in the breccia blocks (with dips ranging from 18° to 77°), but with a dominant dip towards the NNE. On the top of An Dornabac ridge, a widespread breccia overlies a large internally coherent troctolite and peridotite slab. Shearing is recorded at the base of this slab and provides evidence for dynamic movement of the slab as a whole, and indicates derivation from the Western Layered Series (Wadsworth, 1992). The sliding of the slab into the Long Loch Fault graben was followed by major deposition of an angular block mélange that deposited broken-off rock debris on top of the slab (Fig. 5d and e). On the eastern side of the Central Series, the collapse breccias dip with variable inclinations (ranging between 25° to 60°), but with an overall dip-direction towards the WNW and a tendency of steepening towards the Long Loch Fault. The Central Series margin with both the Eastern and Western Layered Series displays intrusion breccias at several localities (Fig. 4b), whereas collapse and slump breccias

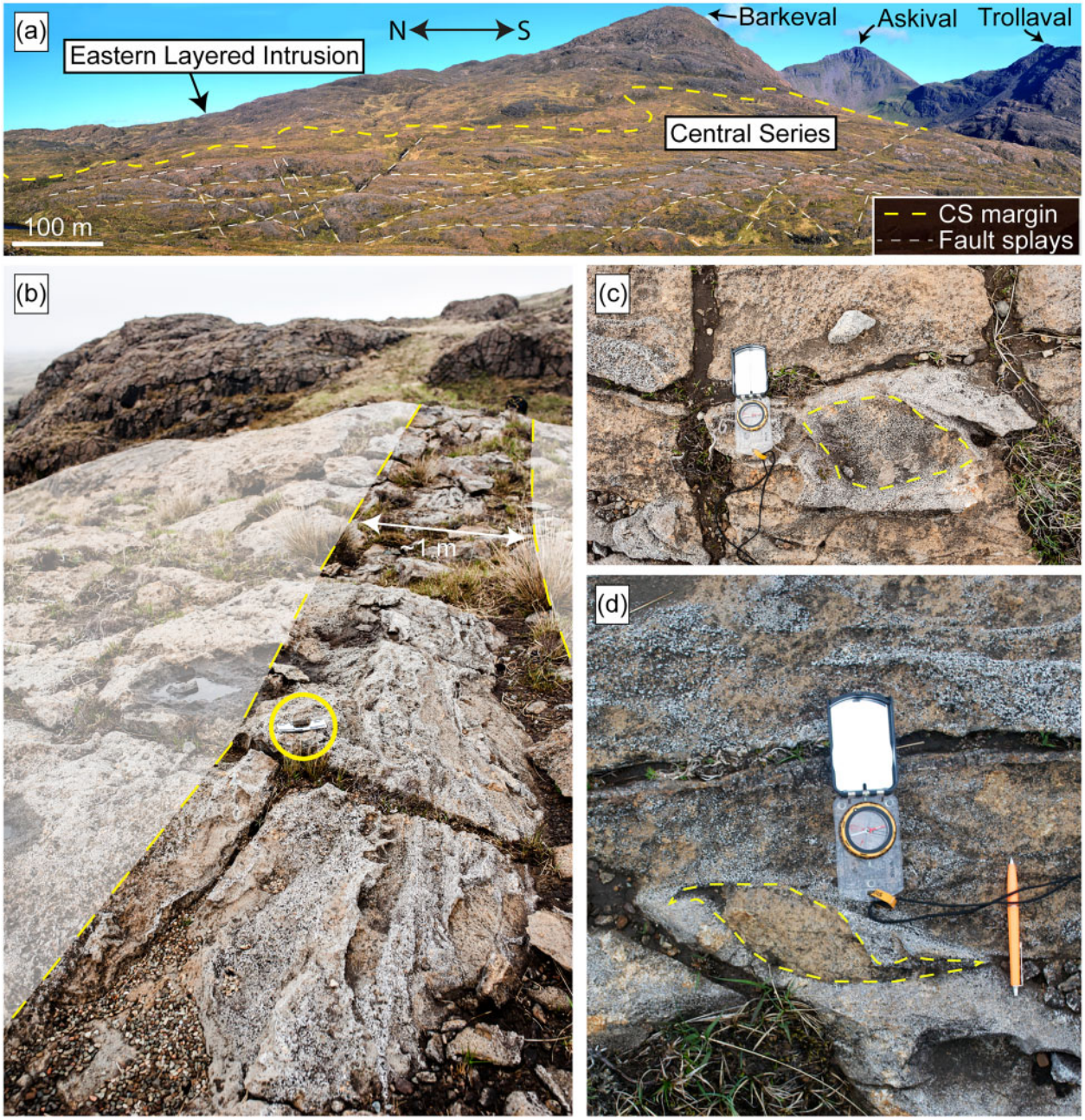

Fig. 9. (a) The eastern portion of the Central Series viewed from west. Dashed white lines mark visible fault splays, while the yellow dashed line represents the approximate margin of the Eastern Layered Intrusion. This marginal zone is highly irregular, due to faulting and associated detachment of layered slabs from the Eastern Layered Series into the Central Series. (b) Example of an N–S oriented shear zone of feldspathic peridotite in the Central Series (≤1 m). Encircled scale-card is 15 cm long. (c) Deformed clast of troctolite in the shear zone shows alignment parallel to the strike of the shear zone. Compass for scale. (d) Sinusoidal peridotite clast in troctolite (grey) with deformed wings (brown with yellow dashed line). Compass for scale.

are very common in the axial central portion of the Central Series (Fig. 4a). The eastern and western margins of the Central Series thus broadly mirror each other.

A well-exposed N–S ridge (informally known as the 'whale-back'; Emeleus & Troll, 2014), located NW of the Long Loch (see Figs 2 and 7a), displays modally layered troctolites traceable for over 500 m The 'whale-back' exposes an abrupt contact between well-layered troctolite and a massive conglomerate-like micro-breccia comprised of partly rounded and in part angular clasts of dunite in a feldspathic peridotitic matrix, with clast sizes up to ~10 cm across that we refer informally to as the 'pebbly' peridotite (Fig. 7b and c). The basal contact to the 'pebbly' peridotite micro-breccia is dipping at ~30° and it appears that the 'pebbly' peridotite covered a pre-existing topography at the chamber floor. The rocks show normal modal grading over the next few metres away from the contact until they become millimtre-sized individual olivine crystals, which

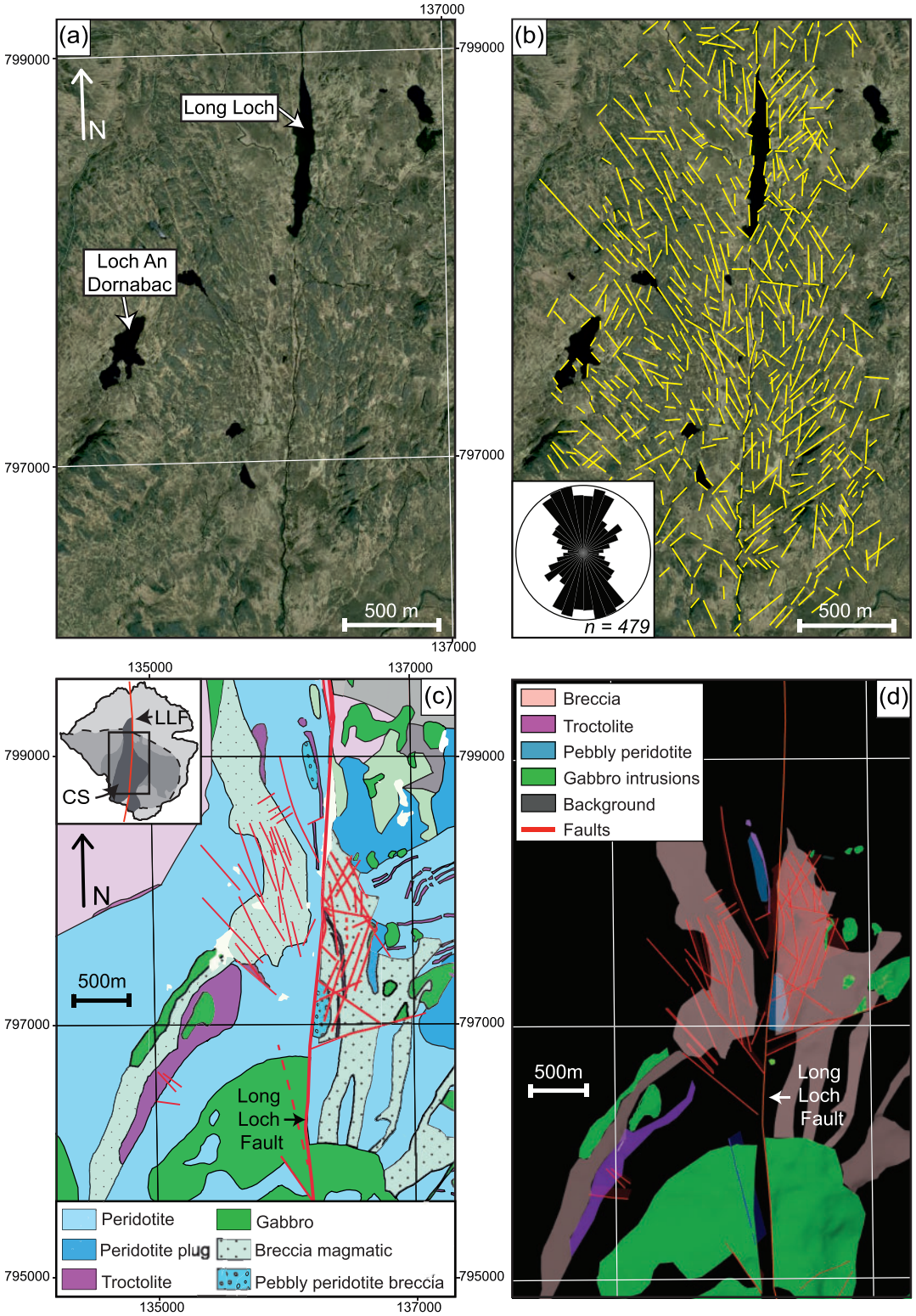

Fig. 10. (a) Unmodified satellite image of the Central Series (source: *Esri, DigitalGlobe*). (b) The same satellite image, but with marked lineaments (yellow lines) assumed to dominantly represent faults. Inset shows bi-directional rose plot (areal scaling, interval size = 10) of Central Series faults detected in the field and determined by remote sensing. Three main groups of faults are identified: (1) NW–SE, (2) NNE–SSW, and (3) NE–SW, with the first being the most dominant one. (c) Sketch map of the northern part of the Central Series (modified after Emeleus, 2004), documenting ~750 m of right-lateral offset on the Long Loch Fault. (d) Reconstruction of key units within the Central Series through removal of the 750 m of post-magmatic right-lateral displacement. Many of the units and structures of the Central Series seem to link up across the Long Loch Fault when post-magmatic fault movement is removed. In fact, fault splays on either side of the Long Loch Fault mirror each other. Also, we note that 'pebbly' peridotite crops out exclusively along the strike of the Long Loch Fault (see text for details).

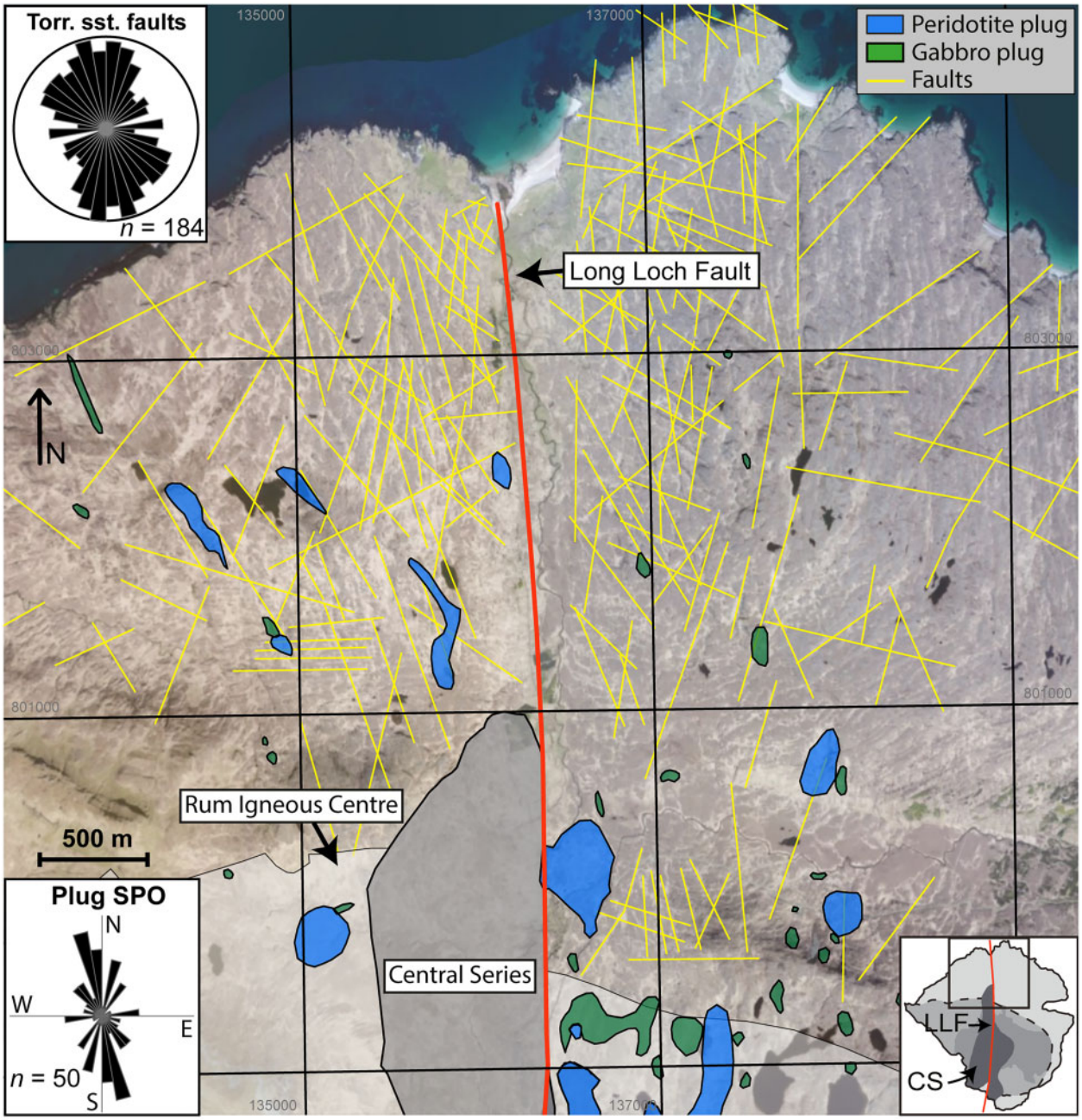

Fig. 11. Satellite image (source: *Esri, DigitalGlobe*) with marked lineaments (yellow lines) and steeply dipping discordant plugs north of the Central intrusion in blue and green (after Emeleus, 2004). Insets show a bi-directional rose plot of lineament orientations (areal scaling, interval size = 10), which we interpret as faults, and SPO (Shape-Preferred Orientation) of the steeply dipping plugs on Rum (linear scaling, max value of 9, interval size = 10). Note the increased density of lineaments closer to the Long Loch Fault and the similarity in orientations between the lineaments that cut the Torridonian sandstone and the preferred orientation of many plugs on Rum (see also **Fig. 10**). This realisation suggests a tectonic control for many of the plugs that show shape-preferred orientations. The relationship between the preferred orientations of the Rum plugs with the orientation of the Long Loch Fault system strengthens the claim that the Long Loch Fault was the primary conduit to the Rum Igneous Centre.

probably represent the suspended smallest fragments that were deposited last. Notably, all outcrops of the 'pebbly' peridotite are dominated by dunite clasts and are positioned in the main topographical low of the Central Series. We therefore deduce that the 'pebbly' peridotite was deposited into an intra magma-chamber depression or graben above the Long Loch Fault. The sorting and erosion of individual olivine grains and pebble-sized peridotite fragments may be explained by gravitational settling into topographic lows in the pluton and the progressively smaller clasts in the 'pebbly' peridotite might reflect several stages of reworking and transport (Fig. 7b) (Mattsson, 2014). This region was marked by upwelling at the active feeder zone(s) along

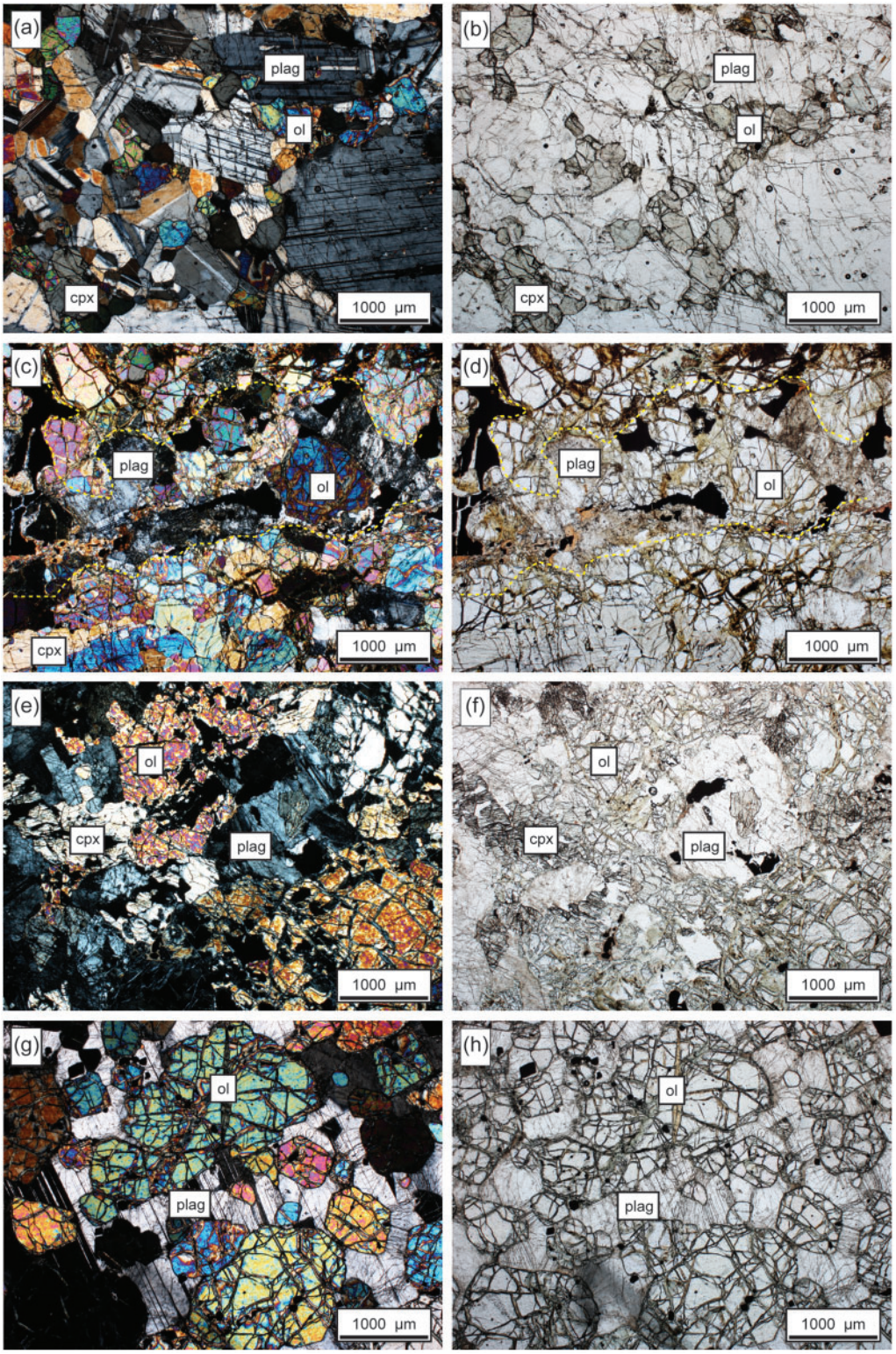

Fig. 12. Microphotographs of rock types in the Central Series. (a) and (b) Gabbro veins. Olivine and clinopyroxene crystals are situated in 'pathways' between larger pyroxenes. Tabular plagioclase crystals are twinned and randomly oriented (CPL and PPL, respectively). (c) and (d) Feldspathic peridotite (breccia matrix) vein intruded into peridotite. The vein contacts are indicated by yellow dashed lines (CPL and PPL, respectively). The veins connect to more voluminous harrisite 'pools' and olivine crystal morphology (c.f. O'Driscoll *et al.*, 2007a), suggest an intricate link between feldspathic peridotite and the harrisite in the Central Series. Note the difference in olivine crystal morphology between panels (c)–(f) and (g)–(j). (e) and (f) Anhedral to subhedral olivine with embayed crystal borders in feldspathic peridotite dyke. Plagioclase crystals comprise the interstices in-between the olivine grains (CPL and PPL, respectively). (g) and (h) Poikilo-macro-spherulitic feldspar texture in 'pebbly' peridotite. Subhedral to euhedral olivine is poikilitically enclosed in plagioclase and clinopyroxene (CPL and PPL, respectively). The olivines (high relief) are unsorted (from 0·1 to 10 mm size) and have different shapes with some crystals showing eroded edges. The olivines also occur in clots.

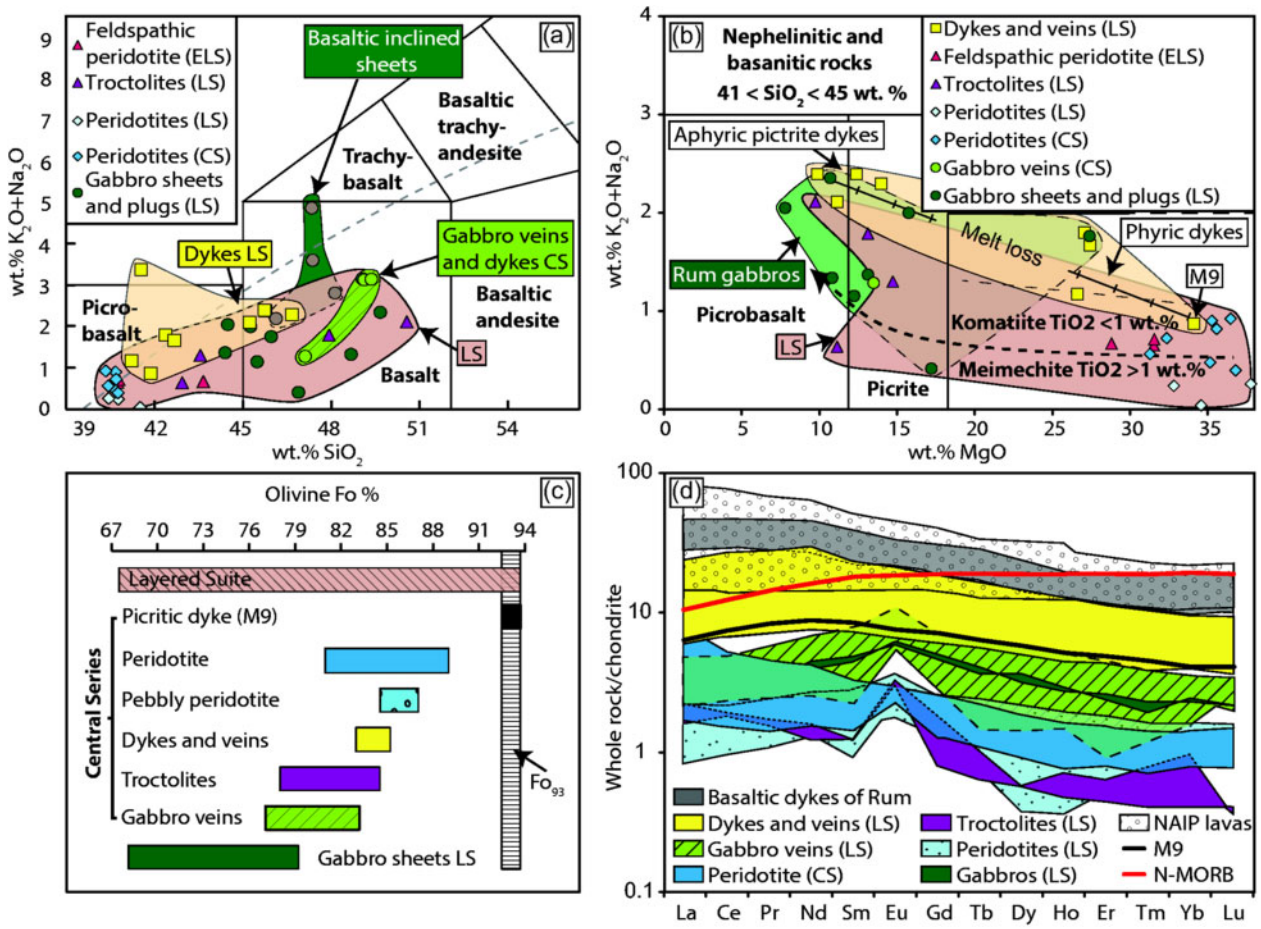

Fig. 13. (a) Total alkali vs silica plot showing data from this work relative to available data for the Layered Suite (LS) and the Central Series (CS) (data from Emeleus, 1997; Upton *et al.*, 2002; Meyer *et al.*, 2009; Leuthold *et al.*, 2014; this study). The Central Series rocks show rather primitive compositions, but progress towards more evolved (gabbroic) composition in the late Central Series dykes and plugs. (b) Classification for mafic rocks after Le Bas (2000) applied to respective Rum lithologies. Dykes and veins in the Central Series (Emeleus, 1997; Upton *et al.*, 2002; Leuthold *et al.*, 2014; this study) classify as komatiitic. (c) Olivine compositions in the various lithologies of the Central Series and in the Rum Layered Suite as a whole (data from Emeleus, 1997; this study). The olivine compositions in the Central Series overlap with those of the Layered Series overall (red bar), but do generally not exceed Fo_{90}, although compositions up to Fo_{93} are known from Rum (grey vertical bar). (d) REE-plot (normalised to chondrite) of the various lithologies of the Layered Suite and the Central Series (data from McDonough & Sun, 1995; Upton *et al.*, 2002; Meyer *et al.*, 2009; Leuthold *et al.*, 2014; this study; Table 3). Reference field for general transitional to enriched LREE lavas of the North Atlantic Igneous Province and for N-MORB are indicated (after Hemond *et al.*, 1988; Sun & McDonough, 1989; Saunders *et al.*, 1997). Whereas Rum basaltic dykes overlap with the NAIP data, the Rum cumulate rocks lost considerable amounts of melt. In turn, the recharging feldspathic peridotite veins and dykelets in the Central Series show trace element concentrations similar to, but slightly lower than the NAIP lavas, which indicates that the Central Series dykelets and veins have lost melt and represent a partial cumulate assemblage.

the Long Loch Fault and was probably influenced by sliding of mega-blocks and slabs at the roof and margins of the Central Series, creating repeated turbulent currents in the magma reservoir (c.f. Wager & Deer, 1939; Wager, 1963; Wager & Brown, 1968; Emeleus *et al.*, 1996; Marsh, 1996).

Lithologies of the Central Series

The lithologies of the Central Series range from dunitic peridotites through feldspathic peridotites to troctolites, wehrlites and gabbros (Fig. 12) (McClurg, 1982; Volker & Upton, 1990; Emeleus, 1997). Previously reported olivine compositions throughout the Layered Suite are $Fo_{93–68}$ (Donaldson, 1975; Dunham & Wadsworth, 1978; Kitchen, 1985; Emeleus, 1997; Upton *et al.*, 2002; Fig. 13), while those for the Central Series are $Fo_{89–74}$ (see Emeleus, 1997). The Mg# in clinopyroxenes in the Central Series is $Mg\#_{86–79}$ and overlaps with $Mg\#_{90–74}$ for the Layered Series as a whole. The reported anorthite (An) content in plagioclase in the Central Series is $An_{85–61}$, which compares to $An_{89–61}$ within the Layered Suite overall (Donaldson, 1975; Dunham & Wadsworth, 1978; Emeleus, 1997; Upton *et al.*, 2002). Olivines in peridotite and dunitic peridotite clasts in the Central Series breccias ($Fo_{89–81}$) and in the 'pebbly' peridotite ($Fo_{87–84}$), however, have generally higher magnesium content than the troctolites ($Fo_{85–78}$; Wadsworth, 1992; Table 2), while olivines in the numerous plagioclase-rich veins and dykelets lie within the range seen in the Central Series peridotite clasts ($Fo_{85–83}$) (Wadsworth,

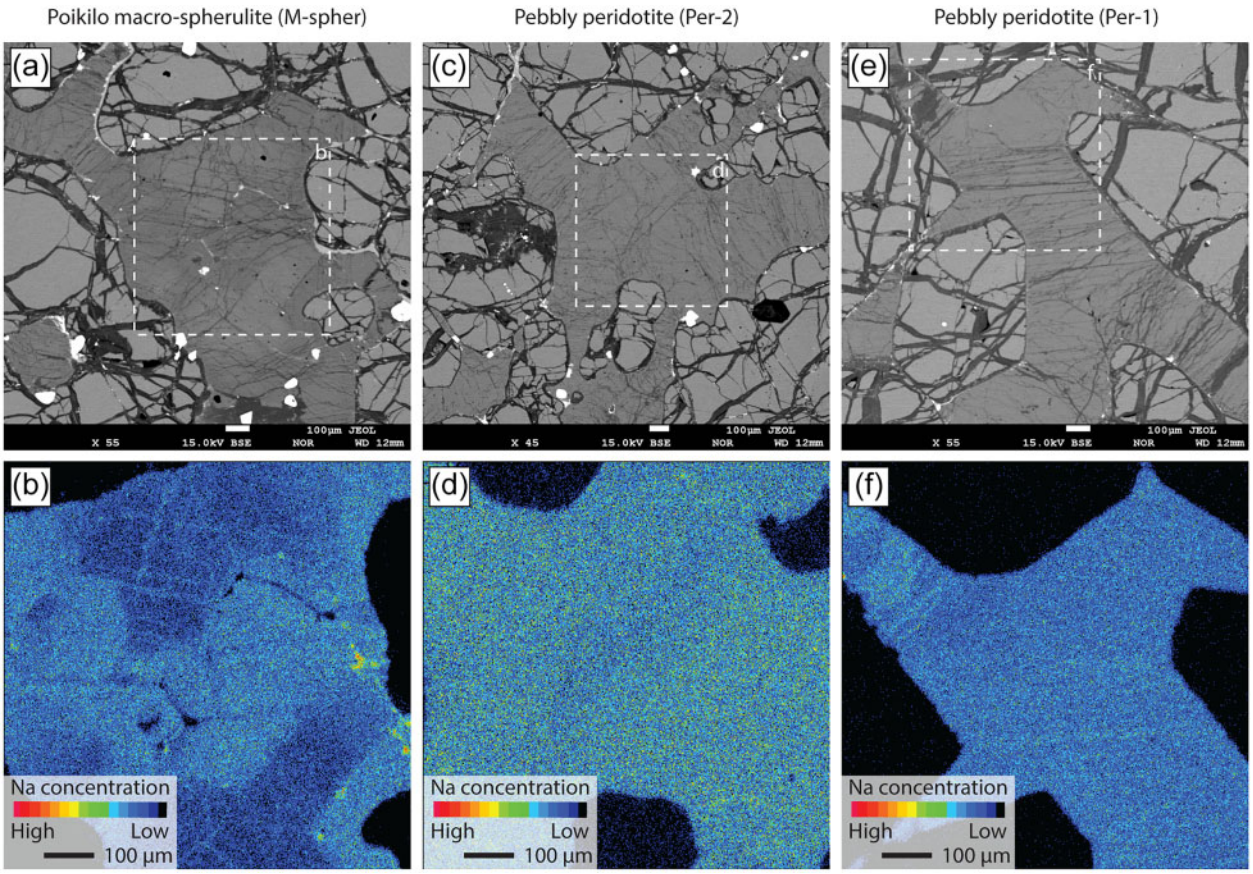

Fig. 14. Element maps of plagioclase in Central Series cumulate peridotites: (a) Back-scattered electron image and (b) Na element map of the plagioclase interstices in poikilo-macro spherulite textured peridotite. The area of the map is indicated by the white (dashed) square. (c) Back-scattered electron image and (d) Na element map of plagioclase interstices in the 'pebbly' peridotite (Per-2). The area of the map is indicated by the white (dashed) square. (e) Back-scattered electron image and (f) Na element map of the plagioclase interstices in 'pebbly' peridotite (Per-1). The area of the map is indicated by the white (dashed) square. The poikilo-macro spherulite textured rock displays zoning, which suggests that it was infiltrated by successive, in part Na and LREE-rich melt parcels likely causing the formation of the poikilo-macro spherulite texture. In contrast, the 'pebbly' peridotite micro-breccia interstitial groundmass is weakly zoned or even devoid of zoning. The 'pebbly' peridotite whole rocks have higher LREE-contents compared to the poikilo-macro spherulite textured rock (c.f. **Fig. 17b**), which suggests that the 'pebbly' peridotite micro-breccia is a mixture of older olivine-rich cumulate (peridotite) fragments and evolved Central Series plagioclase-rich melt.

1961, 1992; McClurg, 1982; Volker, 1983; Emeleus *et al.*, 1996; Emeleus, 1997). Interstitial plagioclase in poikilo-macro-spherulite textured peridotites displays compositional zoning. In contrast, feldspar in the 'pebbly' peridotite interstices is largely un-zoned (Fig. 14). The late gabbro veins have olivine with a range of $Fo_{83–77}$ and thus represent somewhat more evolved basaltic magmas that also recharged the Central Series, showing that both primitive and more evolved magmas replenished the Rum system via the Central Series (Fig. 13c; Table 2). In addition, hydrous minerals, such as kaersutitic amphibole and phlogopite are more abundant in the Central Series, whereas they are in the Eastern Layered Series (c.f. Brown, 1956; Volker, 1983) (Fig. 15). The Central Series rocks are in general much more deuterically altered than the Eastern Layered Series and phlogopite, biotite, and kaersutite have frequently formed from breakdown of clinopyroxene and olivine, and constitute overgrowth rims on oxides (c.f. Donaldson, 1975). Notably, the Eastern Layered Series olivine is commonly fresh and unaltered whereas that in the Central Series displays often distinct alteration (serpentinization) in the fractures in, and boundaries between, the olivine crystals (Fig. 15). Hydrous phases usually occur in association with harrisite textures, poikilo-macro-spherulites and the common replacement 'fingers' in the Central Series (Donaldson *et al.*, 1973; Donaldson, 1975; Butcher *et al.*, 1985; Emeleus, 1997; Holness, 2005; Holness & Winpenny, 2009). On Rum, olivine is often replaced by mica next to intruding feldspathic peridotite veins, which together with interstitial amphibole (e.g. tremolite), and the occurrence of chlorite probably indicates a water-rich nature to the intruded feldspathic peridotite magma(s). These hydrous magmas then reacted with the pre-existing and often feldspar-rich cumulates (Donaldson, 1975).

Pyroxene composition and barometry

The clinopyroxenes in the Central Series record a range of $Mg\#_{86–79}$ (Donaldson, 1975; Dunham & Wadsworth,

Table 2: Representative olivine compositions from the Central Series (full dataset in Supplementary Table 1)

Sample	C-Gabbro1	C-Gabbro1	C-Gabbro2 A	C-Gabbro2 A	Har-dyke 1	Har-dyke 1	Har-dyke2 B	Har-dyke2 B	M- Spher A	M- Spher A	Per2 B	Per2 B
Analysis	ol-1	ol-2	ol-2	ol-3	ol-2	ol-11	ol-1	ol-3	ol-1	ol-2	ol-1	ol-2
Rock type	Gabbro	Gabbro	Gabbro	Gabbro	Feldspathic peridotite	Feldspathic peridotite	Peridotite	Peridotite	Pebbly peridotite	Pebbly peridotite	Pebbly peridotite	Pebbly peridotite
Major elements (wt%)												
SiO_2	40·27	40·39	39·03	39·24	40·38	40·29	39·93	40·19	40·64	40·43	40·04	40·70
FeO	15·87	16·05	20·81	21·30	15·22	15·12	17·37	17·42	13·98	13·88	14·07	13·11
MnO	0·29	0·28	0·35	0·29	0·29	0·32	0·21	0·27	0·22	0·20	0·19	0·20
MgO	44·02	43·87	39·50	39·90	45·03	43·75	42·76	42·77	45·13	45·46	44·93	46·15
CaO	0·06	0·08	0·06	0·04	0·04	0·05	0·05	0·07	0·09	0·12	0·13	0·23
NiO	0·24	0·34	0·23	0·23	0·25	0·25	0·28	0·20	0·29	0·30	0·31	0·41
Cr_2O_3	0·04	0·01	0·01	0·04	–	–	–	0·01	–	0·03	–	0·02
Total	100·79	101·05	100·11	101·10	101·25	99·90	100·74	100·94	100·38	100·57	99·69	100·91
Fo %	83·18	82·97	77·19	76·96	84·06	83·76	81·44	81·40	85·19	85·37	85·06	86·26

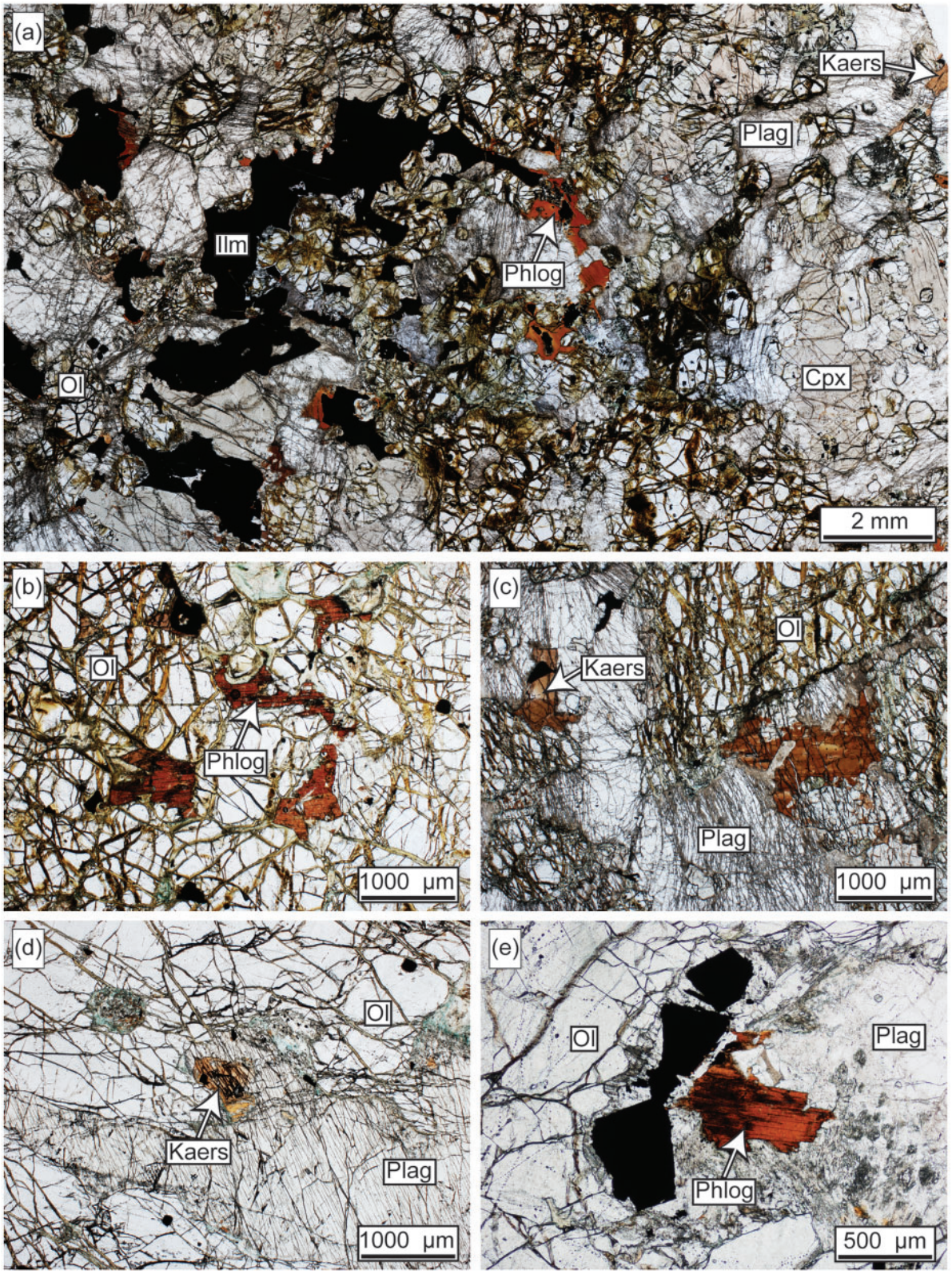

Fig. 15. (a) Photomicrograph of typical occurrence of phlogopite (red), kaersutite (brown) and abundant ilmenite (black) in a feldspathic peridotite vein in the Central Series (PPL). (b) Common interstitial phlogopite (red to brown) in 'pebbly' peridotite, Central Series (PPL). (c) Photomicrograph of abundant phlogopite (red) and kaersutite (brown) in a feldspathic peridotite dyke, Central Series (PPL). (d) Typical occurrence of kaersutite (light brown) in peridotite of the Barkeval plug that intruded the Eastern Layered Series (PPL). (e) Phlogopite (red) in alteration zone in the peridotite of the Barkeval plug, Eastern Layered Series (PPL). Note that in plates (a), (b), (c) the olivines are much more deuterically altered than in (d) and (e). Further, there are marked differences in alteration of olivine and pyroxene between the Central Series rocks (a)–(d) and the Barkeval plug rocks (e), (f).

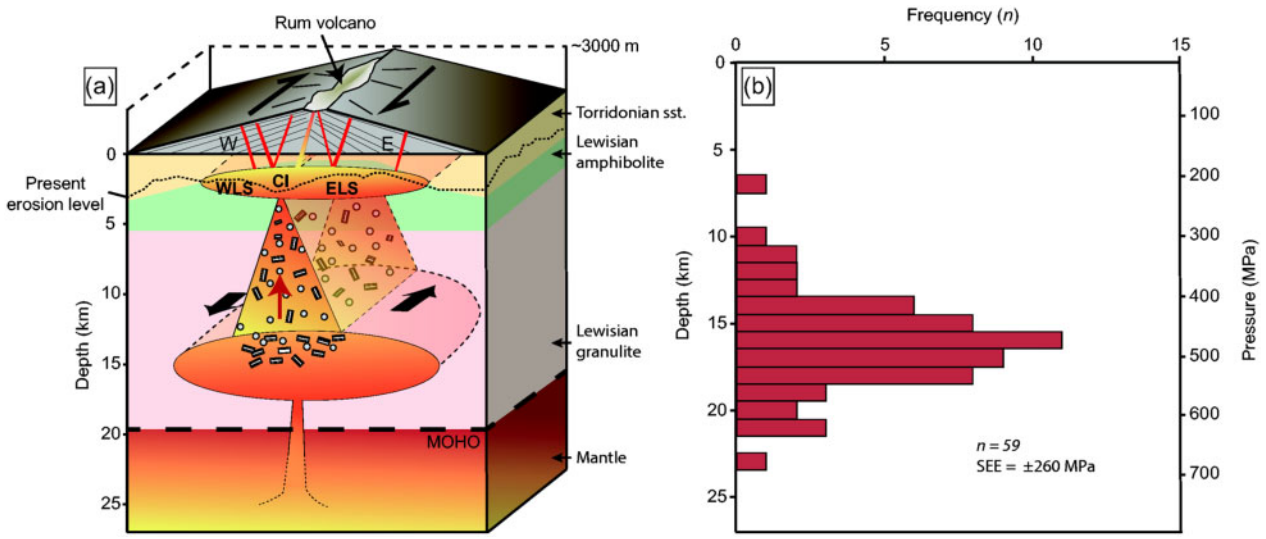

Fig. 16. (a) Magma supply system to the Rum Layered Suite based on (b) barometry of Central Series clinopyroxene crystals, after Nimis (1995) and Putirka (2008). The crustal stratigraphy of the Hebridean Terrane below Rum is from Park *et al.* (2002). The Long Loch Fault probably connected the shallow Rum magma chamber system with a deeper holding chamber and we envisage that the Long Loch Fault repeatedly opened and closed the magma pathway, thus modulating pressure build-up in the deeper magma reservoir. Major layered units in the Rum Layered Suite may then reflect fault movement and pressure release that caused considerable volumes of crystal- and H_2O-rich magmas to ascend rapidly from depth. When arriving in the shallow reservoir, the dense crystal-laden magmas intruded existing cumulates and also deposited their crystal load onto the reservoir floor to produce rhythmic cumulate layers.

1978; McClurg, 1982; Emeleus, 1997; Upton *et al.*, 2002; this study) and are diopsides grading to augites according to the scheme of Morimoto (1988). The larger clinopyroxene phenocrysts from the gabbro veins are zoned and the rims have marginally lower Mg# ($Mg\#_{84–79}$) compared to the cores (Fig. 12). To constrain the volcanic supply system to the Rum Igneous Complex, clinopyroxene barometry was employed, which uses major element clinopyroxene mineral data (from EMP). We applied the Nimis (1995) geobarometer, as modified by Putirka (2008, eqn. 32b) to gabbro veins and feldspathic peridotite dyke samples. This barometer estimates pressure of clinopyroxene crystallization on the basis of the cation fractions in the clinopyroxene unit cell. Equation 32b accounts also for H_2O content of the parent magma as well as temperature of crystallization (Putirka, 2008). The H_2O content was set to 2·5 wt % and the temperature input was set to 1200° C, following crystallization temperature estimates of the Central Series breccia matrix by Donaldson (1975). The standard error of estimate (SEE) for this barometer is ±260 MPa (Putirka, 2008).

Pyroxene phenocrysts from the gabbro veins (*n* = *37*) yield crystallization pressures of between 280 and 600 MPa (SEE ±260 MPa), corresponding to between c.10 to 20 km depth. Clinopyroxene in feldspathic peridotite dykes (up to 1 mm in diameter; *n* = *22*) crystallized at pressures between 180 and 650 MPa (SEE ±260 MPa), corresponding to a depth range of ~6–22 km assuming mafic rock as the dominant overburden lithology. Allowing for the relatively large uncertainties, it is noteworthy that none of the calculated clinopyroxene crystallization pressures show a shallow depth of equilibration and all sample groups record pressures >10 km. Therefore, many of the clinopyroxene crystals may not have formed *in situ*, but were probably brought in with migrating magma as crystal cargo (Fig. 16).

Magmatic water contents in the Central Series

All analysed clinopyroxenes showed absorption maxima at 3630, 3530, and 3460 cm^{-1} in the IR spectra, corresponding to the typical vibrational bands expected for OH in diopside (e.g. Skogby, 2006). The OH band at around 3630 cm^{-1} is prominent for E||α and E||β, while the two bands around 3530 and 3460 cm^{-1} dominate for E||γ. This infra-red pleochroic behaviour is typical for clinopyroxene OH bands (e.g. Beran, 1976) and thus excludes the influence of possible OH-bearing impurities (e.g. hydrous minerals, melt/fluid inclusions). No hydrogen diffusion profiles were observed in the analysed clinopyroxene crystals. The analysis on pyroxene crystals from the gabbro veins (*n* = *7*) yielded 295–336 ppm H_2O in the crystals. When converted to magma H_2O contents, following the procedure in O'Leary *et al.* (2010) and Weis *et al.* (2015), the original water content of the gabbro vein magma is calculated to range between 2·0 and 3·4 wt % (±0·6) H_2O (Table 1), which is remarkably high for regular North Atlantic Igneous Province (NAIP) magmas (but compare Gillis *et al.*, 2014*a*).

Major and trace elements

The rocks of the Central Series range from dunitic peridotite to gabbro and the breccia matrix compositions

also range from peridotite to gabbro. The Central Series cumulates are all relatively primitive, with high Mg# (>80) for the peridotites, and >75 for the gabbros (c.f. Gillis *et al.*, 2014*a*; Nozaka *et al.*, 2017). The higher Mg# values in the poikilo-macro-spherulitic peridotites are coupled with lower Ca# relative to those from e.g. bulk rocks from the Eastern Layered Series peridotites. This can potentially be explained by subtraction (fractionation) of plagioclase with little to no accompanying clinopyroxene. Alternatively, later addition of evolved (low Ca) plagioclase-rich liquid into the cumulate pile could have occurred, which would be consistent with relatively high average REE concentrations for these samples compared to other samples from the Layered Suite (Fig. 17a and b). With the exception of one significantly more evolved dyke (Dyke-RM2), the feldspathic peridotite dykes (e.g. samples Har-dyke 1A and 1B; Table 3) have similar Mg# and Ca#s to the most evolved Central Series gabbro. The intruding feldspathic peridotite veins and dykelets have high MgO contents (Fig. 13a and b). The REE pattern for the feldspathic peridotite veins and dykelets relative to MORB shows close resemblance to the primitive 'Transitional-to-Enriched' type tholeiitic basalts of the NAIP with a maximum enrichment in Nd, but a small depletion of La with respect to Ce and Nd (Fig. 13d). The komatiitic nature of the feldspathic peridotite dykes and veins as well as their REE patterns lie between average NAIP basalt and the basaltic dykes of Rum on the one side, and the Rum cumulate compositions on the other, which points to a degree of melt loss from these compositions (c.f. Holness *et al.*, 2007; Leuthold *et al.*, 2014, 2015). However, the REE pattern of the Central Series cumulate peridotites are somewhat enriched in LREE relative to the Eastern Layered Series peridotites, which have convex REE curves with Eu peaks. The REE concentrations of the Central Series peridotites are more similar to those of the Eastern Layered Series troctolites (plagioclase-rich cumulate) than to their peridotites (Fig. 17b). Additionally, the higher concentrations of REE within the gabbroic veins in the Central Series (up to 3 x chondritic for the HREE, compared to about 1·5 x in the cumulate peridotites) are in part a reflection of a melt fraction present, but probably also indicate that the Central Series gabbros likely crystallized from more REE-enriched and thus more evolved melts than did, for example the ELS cumulates.

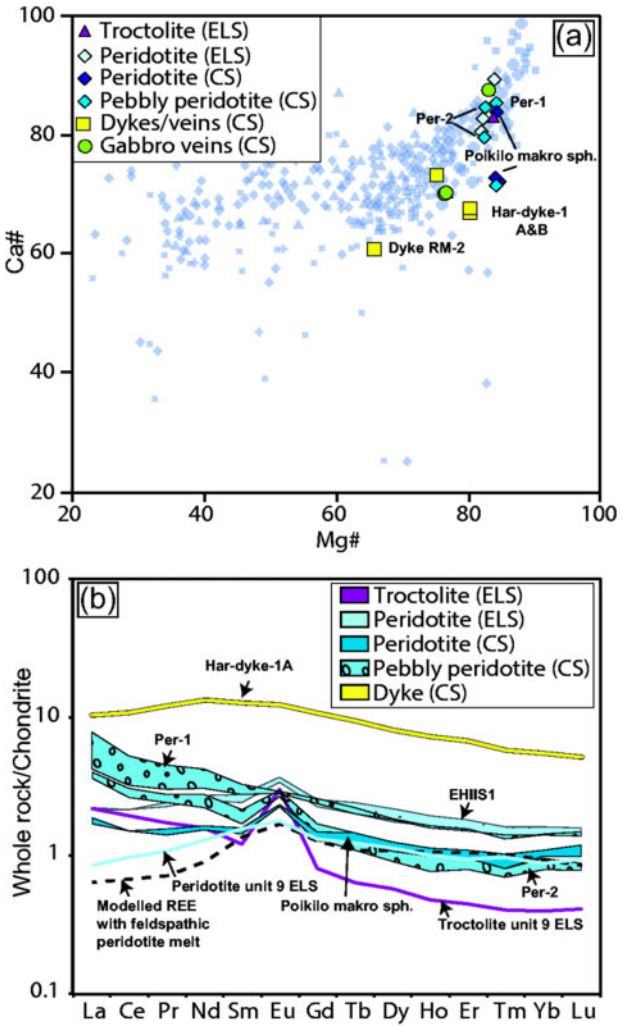

Fig. 17. (a) Correlation of Ca# and Mg# of representative samples of harrisitic peridotite vein, magnesium-rich dykes, peridotites, troctolites, gabbro veins, and poikilo-macro-spherulithic plagioclase peridotites from the Central Series on Rum. The Mg# (100 x Mg/(Mg +Fe)) and Ca# (100 x Ca/(Ca + Na)) of all samples, except Dyke-RM 2, show that these rocks are primitive relative to fast spreading lower oceanic crustal rocks (light blue reference samples from Gillis *et al.*, 2014b and references therein). The low Ca# of the poikilo-macro-spherulitic plagioclase peridotite is likely a result of presence or later infiltration of evolved alkaline fluids and melts (e.g. from more evolved feldspathic peridotite dykes and veins). (b) REE plot of Central Series peridotites compared to peridotite and troctolite from the Eastern Layered Series (ELS). The black dashed line shows the modelled REE pattern of a cumulate rock calculated via a Rayleigh fractionation model from a primary melt identical to the feldspathic peridotite dykes (Har-dyke 1A) using 80% solidification of an olivine (0·7), plagioclase (0·2) and clinopyroxene (0·1) assemblage. The modelled REE pattern follows the measured pattern for the Eastern Layered Series Unit 9 peridotite well (normalizing values from McDonough & Sun, 1995 and modelling parameters from Meyer *et al.* 2009). The Central Series cumulate peridotites, on the other hand, are enriched in LREE compared to the Eastern Layered Series (ELS) peridotites and display REE patterns more similar to troctolite. Assuming the Central Series cumulate peridotites initially had REE compositions similar to the Eastern Layered Series peridotites, post-cumulus interaction/mixing between plagioclase-rich melt and the Central Series cumulate peridotites is inferred. Reference data in (a) and (b) from the Eastern Layered Series are from Emeleus (1997) and Meyer *et al.* (2009).

DISCUSSION

Three-dimensional geometry of the Central Series

The 3 D-projection in connection with structural and lineament observations in the Central Series imply that strike-slip movement was a key factor during formation of the Central Series. When reconstructing post-magmatic right-lateral fault movement along the Long

Table 3: Major and trace element data on Central Series and Rum Igneous Complex

Sample	Har-dyke 1A	Har-dyke 1B	Per1 A	Per1 B	Per2 A	Per2 B	Per-Har-Vein	M-Spher A	M-Spher B	C-Gabbro1	C-Gabbro2 A	C-Gabbro2 B
Location	East of Long Loch CS	East of Long Loch CS	Whale-Back	Whale-Back	Close to LLF	Close to LLF	Eastern CS	South of Long Loch	South of Long Loch	South of Long Loch	Eastern CS	Eastern CS
GR	36494	36494	36226	36226	36287	36287	36548	36368	36368	36314	36474	36474
(all NM)	98240	98240	98762	98762	97270	97270	97774	97851	97851	97907	97543	97543
Rock type	Feldspathic peridotite	Feldspathic peridotite	Pebbly peridotite	Pebbly peridotite	Pebbly peridotite	Pebbly peridotite	Feldspathic peridotite	Peridotite	Peridotite	Gabbro	Gabbro	Gabbro
Major elements (wt %)												
SiO_2	42·37	42·67	40·34	40·76	40·69	40·42	41·21	40·64	40·67	47·10	49·11	49·35
TiO_2	1·00	1·00	0·24	0·26	0·17	0·19	1·91	0·18	0·17	0·47	0·46	0·47
Al_2O_3	7·87	7·70	4·26	4·10	8·10	7·93	6·01	5·39	5·81	15·72	17·86	18·39
Fe_2O_3	12·79	13·03	13·24	13·36	13·37	12·78	17·05	12·78	12·89	5·32	5·71	5·69
MnO	0·22	0·22	0·23	0·23	0·22	0·21	0·30	0·22	0·23	0·11	0·11	0·11
MgO	27·08	27·43	36·50	36·81	32·38	31·31	26·62	35·18	35·29	13·54	9·65	9·46
CaO	6·17	6·04	4·00	3·97	4·86	5·41	5·31	4·32	4·17	15·90	13·10	13·07
Na_2O	1·68	1·57	0·87	0·37	0·68	0·54	1·07	0·46	0·85	1·24	3·02	3·05
K_2O	0·12	0·10	0·06	0·03	0·05	0·03	0·10	0·02	0·05	0·04	0·11	0·10
P_2O_5	0·04	0·04	0·02	0·02	0·02	0·02	0·02	0·02	0·02	0·01	0·01	0·02
Total	99·34	99·80	99·73	99·90	100·53	98·84	99·59	99·21	100·15	99·46	99·14	99·71
Trace elements (ppm)												
Li	9·73	2·09	1·87	1·87	2·13	2·30	2·50	1·76	4·03	2·19	2·14	1·98
Sc	21·85	21·79	16·22	15·55	10·29	11·61	24·39	12·24	13·54	44·42	32·30	31·25
V	176·85	175·01	81·57	78·17	63·04	59·62	216·11	68·39	69·88	141·87	142·58	132·84
Cr	2092·11	2154·27	2908·86	2721·27	2936·65	2588·68	538·74	2832·07	2809·95	1977·43	739·03	684·17
Mn	1209·57	1244·98	1226·22	1215·49	1220·92	1118·37	1630·03	1228·26	1218·69	592·99	639·86	610·14
Co	101·62	103·70	130·24	128·68	123·92	110·64	126·95	128·29	127·88	40·41	38·02	36·63
Ni	1228·58	1254·10	1733·86	1728·49	1522·08	1370·59	916·56	1566·94	1559·14	499·85	349·78	336·45
Cu	28·30	27·06	25·59	36·37	70·59	61·70	94·26	89·19	84·53	50·87	174·24	169·91
Zn	70·48	72·63	92·77	71·90	72·39	64·89	90·84	68·67	68·53	25·88	30·37	29·27
Rb	1·15	1·23	0·23	0·21	0·57	0·14	1·34	0·08	0·08	0·28	0·52	0·58
Sr	143·62	143·91	59·68	60·15	125·67	128·46	103·25	72·24	67·63	194·30	309·56	309·26
Y	9·41	9·41	2·25	2·11	1·10	1·34	5·94	1·32	1·51	6·09	6·53	6·29
Zr	47·32	47·17	6·39	5·99	2·81	3·21	33·14	2·89	3·13	13·82	12·48	12·03
Nb	0·96	0·96	0·13	0·11	0·13	0·04	2·57	0·04	0·03	0·15	0·09	0·10
Cs	0·02	0·02	0·01	0·00	0·01	0·00	0·02	0·00	0·00	0·00	0·01	0·01
Hf	1·46	1·47	0·23	0·22	0·11	0·13	1·02	0·10	0·12	0·57	0·52	0·50
Pb	0·42	0·46	0·88	0·22	0·28	0·26	0·68	0·14	0·14	0·21	0·49	0·51
Th	0·16	0·15	0·02	0·02	0·00	0·00	0·11	0·01	0·00	0·02	0·02	0·02
U	0·04	0·04	0·01	0·01	0·00	0·00	0·03	0·00	0·00	0·01	0·01	0·01
La	2·47	2·45	1·84	1·00	0·86	0·95	1·66	0·45	0·40	1·02	1·14	1·11
Ce	6·64	6·66	3·22	1·99	1·62	1·87	4·12	0·93	0·92	2·73	2·99	2·93
Pr	1·12	1·15	0·42	0·28	0·23	0·26	0·66	0·13	0·15	0·49	0·54	0·52
Nd	6·10	6·22	1·93	1·41	1·02	1·26	3·45	0·71	0·75	2·90	3·13	2·98
Sm	1·88	1·91	0·49	0·41	0·25	0·32	1·08	0·21	0·23	1·03	1·14	1·07
Eu	0·69	0·69	0·17	0·16	0·15	0·17	0·43	0·13	0·13	0·48	0·61	0·60

(continued)

Table 3: Continued

Sample	Har-dyke 1A	Har-dyke 1B	Per1 A	Per1 B	Per2 A	Per2 B	Per-Har-Vein	M-Spher A	M-Spher B	C-Gabbro1	C-Gabbro2 A	C-Gabbro2 B
Location	East of Long Loch CS	East of Long Loch CS	Whale-Back	Whale-Back	Close to LLF	Close to LLF	Eastern CS	South of Long Loch	South of Long Loch	South of Long Loch	Eastern CS	Eastern CS
GR	36494	36494	36226	36226	36287	36287	36548	36368	36368	36314	36474	36474
(all NM)	98240	98240	98762	98762	97270	97270	97774	97851	97851	97907	97543	97543
Rock type	Feldspathic peridotite	Feldspathic peridotite	Pebbly peridotite	Pebbly peridotite	Pebbly peridotite	Pebbly peridotite	Feldspathic peridotite	Peridotite	Peridotite	Gabbro	Gabbro	Gabbro
Gd	2·13	2·10	0·52	0·47	0·26	0·34	1·21	0·25	0·29	1·29	1·39	1·34
Tb	0·34	0·34	0·08	0·07	0·04	0·05	0·20	0·04	0·05	0·21	0·23	0·22
Dy	2·02	2·04	0·46	0·44	0·22	0·28	1·23	0·26	0·31	1·30	1·40	1·36
Ho	0·39	0·40	0·09	0·09	0·04	0·06	0·24	0·05	0·06	0·26	0·28	0·27
Er	1·05	1·07	0·25	0·24	0·13	0·15	0·70	0·15	0·17	0·69	0·72	0·70
Tm	0·14	0·14	0·03	0·03	0·02	0·02	0·09	0·02	0·02	0·09	0·09	0·09
Yb	0·87	0·88	0·23	0·22	0·13	0·15	0·64	0·16	0·17	0·52	0·57	0·57
Lu	0·13	0·13	0·04	0·03	0·02	0·02	0·10	0·02	0·03	0·07	0·08	0·08

Sample	Per-RM1	Dyke-RM2	EHIIS1 A	EHIIS1 B	DU 23767	DU 23768	DU 23769	R-CS-U
Location	East of Long Loch CS	East of Long Loch CS	ELS Unit 5	ELS Unit 5	Allt Slugain a' Choilich	Allt Slugain a' Choilich	Allt Slugain a' Choilich	Allt Slugain a' Choilich
GR	36494	36494	39877	39877	39449	39401	39509	39601
(all NM)	98240	98240	96959	96959	98589	98468	98768	98995
Rock type	Peridotite	Feldspathic peridotite	Feldspathic peridotite	Feldspathic peridotite	Basalt	Basalt	Basalt	Basalt
Major elements (wt %)								
SiO_2	40·265	41·541	40·73	40·78	46·12	48·11	47·36	47·33
TiO_2	0·28	2·31	0·27	0·26	1·42	1·49	1·66	2·45
Al_2O_3	5·933	11·807	6·27	6·84	14	14·81	14·21	13·31
Fe_2O_3	12·568	16·211	13·26	13·38	11·91	11·74	12·41	14·8
MnO	0·216	0·23	0·22	0·22	0·19	0·17	0·19	0·21
MgO	35·565	15·995	31·55	31·57	10·71	7·83	7·21	5·76
CaO	3·592	9·087	5·35	5	9·81	10·62	10·83	9·07
Na_2O	0·76	3·21	0·61	0·66	1·87	2·56	3	3·43
K_2O	0·059	0·166	0·04	0·05	0·3	0·23	0·58	1·42
P_2O_5	0·021	0·06	0·02	0·01	0·11	0·12	0·13	0·21
Total	99·26	100·61	98·33	98·77	96·44	97·68	97·58	97·99
Trace elements (ppm)								
Li	3·00	2·32	2·53	2·56	–	–	–	–
Sc	9·90	23·11	14·02	16·6	28	30	38	34
V	86·52	273·60	104·48	122·33	294	317	364	463
Cr	4466·96	844·98	4078·79	4181·32	–	–	–	–
Mn	1279·24	1324·45	1264·21	1255·94	–	–	–	–
Co	131·75	85·16	128·94	125·75	62·3	49·6	48·6	49·5
Ni	2259·36	718·47	1675·52	1582·41	205·2	94·9	58·3	41·6
Cu	65·93	38·47	326·31	301·39	143·3	146	159·8	132·1
Zn	72·45	85·02	77·28	77·24	48	47	50	68
Rb	0·44	0·92	0·54	0·41	11·1	8	28	70·8
Sr	74·52	335·29	93·54	89·32	212·7	230·2	280·4	367·1
Y	2·34	11·04	2·12	2·58	18·1	20·8	23·6	29·6
Zr	8·09	67·84	5·04	7·58	97	115·2	109·4	171·5
Nb	0·15	0·73	0·16	0·16	2·9	2·9	2·5	4·6

(continued)

Table 3: Continued

Sample	Per-RM1	Dyke-RM2	EHIIS1 A	EHIIS1 B	DU 23767	DU 23768	DU 23769	R-CS-U
Location	East of Long Loch CS	East of Long Loch CS	ELS Unit 5	ELS Unit 5	Allt Slugain a′ Choilich	Allt Slugain a′ Choilich	Allt Slugain a′ Choilich	Allt Slugain a′ Choilich
GR	36494	36494	39877	39877	39449	39401	39509	39601
(all NM)	98240	98240	96959	96959	98589	98468	98768	98995
Rock type	Peridotite	Feldspathic peridotite	Feldspathic peridotite	Feldspathic peridotite	Basalt	Basalt	Basalt	Basalt
Cs	0·01	0·01	0·01	0·01	1·6	0·6	1·6	5·8
Hf	0·20	1·81	0·19	0·24	2·6	3·1	2·9	4·4
Pb	1·47	0·33	0·65	0·47	0·9	1·7	0·3	0·7
Th	0·05	0·04	0·03	0·08	0·6	1	0·4	0·9
U	0·01	0·01	0·01	0·02	0·2	0·3	$<$0·1	0·2
La	0·55	2·54	0·52	0·51	7	8·1	6·6	11
Ce	1·78	10·51	1·32	1·32	18·2	20·8	17·6	28·5
Pr	0·26	1·92	0·21	0·22	2·66	3·03	2·72	4·34
Nd	1·53	12·57	1·14	1·24	11·9	14·1	13·5	20·6
Sm	0·39	3·30	0·36	0·41	3·33	3·78	3·73	5·68
Eu	0·19	1·16	0·19	0·21	1·21	1·3	1·34	1·85
Gd	0·45	3·21	0·45	0·51	3·8	4·34	4·4	6·1
Tb	0·07	0·46	0·07	0·09	0·61	0·71	0·76	1·02
Dy	0·43	2·48	0·43	0·54	3·41	3·96	4·49	5·66
Ho	0·10	0·51	0·09	0·11	0·7	0·76	0·85	1·06
Er	0·26	1·17	0·25	0·29	1·86	2·03	2·39	3·07
Tm	0·04	0·16	0·03	0·04	0·26	0·29	0·34	0·45
Yb	0·21	0·67	0·22	0·26	1·55	1·67	2·07	2·61
Lu	0·04	0·12	0·03	0·04	0·25	0·27	0·33	0·41

Loch Fault, the fault splay patterns and the main rock-types of the Western and Eastern Central Series broadly link up (Fig. 10), and define the shape of a transtensional graben structure. These structures presumably converge to a 'master' strike–slip fault at depth and the observed arrangement of fault splays and plugs inside the Central Series and in the Torridonian sandstone north of the Central Series define the Long Loch Fault as the former focal zone of magma upwelling for the Rum Layered Suite (Figs 10 and 11). This is in line with studies elsewhere which suggested that tectono-magmatic interactions in strike–slip settings generate conjugate fracture/fault patterns and usually a transtensional basin (c.f. Girard & van Wyk de Vries, 2005; Holohan *et al.*, 2008; Mathieu & van Wyk de Vries, 2011; Mathieu *et al.*, 2011). These inferences support the concept that the Long Loch Fault modulated magma ascent into the Rum magma reservoir (c.f. Donaldson, 1975; Emeleus 1996; Fig. 18), and points to the fault system as the key to understanding the pulsatory (or rhythmic) emplacement of the Layered Suite.

The magma compositions of the Central Series

The Central Series cumulates are compositionally similar to the rocks exposed in the Eastern and Western Layered Series and the clasts in the Central Series breccias are probably dominantly derived from these units (Fig. 13). However, wehrlite cumulates described by Volker & Upton (1990) on Ruinsival are unique within the Layered Suite, and either represent materials (variably sized blocks) derived from now eroded layers higher up in the Layered Series or reflect replacement of interstitial melt similar to what has been proposed, for example the vertical wehrlite pipes of Unit 9 of the Eastern Layered Series (e.g. Leuthold *et al.*, 2014).

The low REE abundances of the peridotites, troctolites, gabbros and poikilo-macro-spherulitic plagioclase peridotites relative to NAIP basalts and basaltic dykes on Rum, attest to the olivine-rich and adcumulus nature of these rocks, reflecting the expulsion of intercumulus melt (c.f. Meyer *et al.*, 2009). The intruding gabbro and feldspathic peridotite veins and dykelets compositionally overlap with the cumulates of the Layered Suite for major elements, but also extend to higher alkalinity and REE concentrations in whole rocks and to lower Fo content in olivine (Fig. 13), which is indicative of more evolved magma that arrived from depth. The pyroxenes in these veins record variable crystallization pressures (depths) in the crust below the evolving Rum Igneous Complex (Fig. 16), suggesting a system of holding chambers or melt pockets existed at depth from which the intrusive pulses where supplied, similar perhaps to what is seen today for many Icelandic volcanoes (c.f. Emeleus & Troll 2014). When considering the trace element pattern further, the cumulate nature of the Central Series samples is emphasised by the lower concentrations relative to common NAIP lavas and also relative to the basaltic cone sheets on Rum (see Emeleus, 1997), which are likely to represent the residual basaltic magmas expelled from the Rum reservoir system. To then explain the observed trace element patterns of the Central Series veins and dykelets, we must consider that they were either losing melt during final emplacement or have picked up previously solidified minerals at depth (Fig. 13b). The REE patterns for the Eastern Layered Series peridotite cumulates can be reproduced with a Rayleigh fractionation model from a primary melt compositionally identical to the feldspathic peridotite dykes (Fig. 17b) (for full descriptions regarding the model calculation, see Meyer *et al.*, 2009). Furthermore, the relatively low concentration of LREEs in olivine implies that fractionation of olivine was unlikely to have contributed to the enriched trace-element pattern of the Central Series cumulate peridotites and instead supports post-cumulus interaction with LREE-rich melts (c.f. Meyer *et al.*, 2009).

Pyroxenes in the Central Series veins and dykelets indicate that at least some of the recharge magma in the Central Series was H_2O-rich with up to 3·5 wt % H_2O, which is consistent with textural and mineralogical observations that show that the Central Series rocks carry more hydrous minerals than those in the other layered Series (Donaldson *et al.*, 1973; Donaldson, 1975; Fig. 15). As a comparison, the water content in Icelandic and NAIP magmas ranges up to ~1·1 wt % H_2O (Jamtveit *et al.*, 2001; Nichols *et al.*, 2002), which compares to a range of up to 1·5 wt % H_2O for ocean island basalts and up to 1·0 wt % H_2O for MORB (see Kovalenko *et al.*, 2007; Weis *et al.*, 2015). In other parts of the Rum igneous complex, alteration phases have been considered to indicate hydrothermal activity involving external fluids (e.g. Greenwood *et al.*, 1992; Holness & Winpenny, 2009). However, on the basis of $\delta^{18}O$ ratios Greenwood *et al.* (1992) and Emeleus (1997) argued that circulating meteoric water had interacted with the Layered Suite mainly at its borders and considerably less so in the central parts of the pluton (see also Kitchen, 1985). This accords with Donaldson's (1975) conclusion that hydrous recharge magmas, rising from depth, were generally responsible and probably the main cause for the more abundant hydrous mineral phases in the Central Series relative to most other portions of the Rum Layered Suite.

Fluid-rock interaction in the Central Series

Modification of the cumulate pile in the Eastern Layered Series by reactive liquid flow locally caused modification of primary compositions and textures (e.g. Butcher, 1985; Bédard *et al.*, 1988; Holness *et al.*, 2007; O'Driscoll *et al.*, 2010; Leuthold *et al.*, 2014, 2015, Hepworth *et al.* 2020*b*). In the Central Series rocks we observe recrystallization, hydrous mineral rim-growth and replacement of pre-existing mineral phases (Figs 12, 14 and 15), all of which are indicative of reaction with hydrous melt (c.f. Beard *et al.*, 2004). Extensive reaction in the Central Series cumulates was most probably

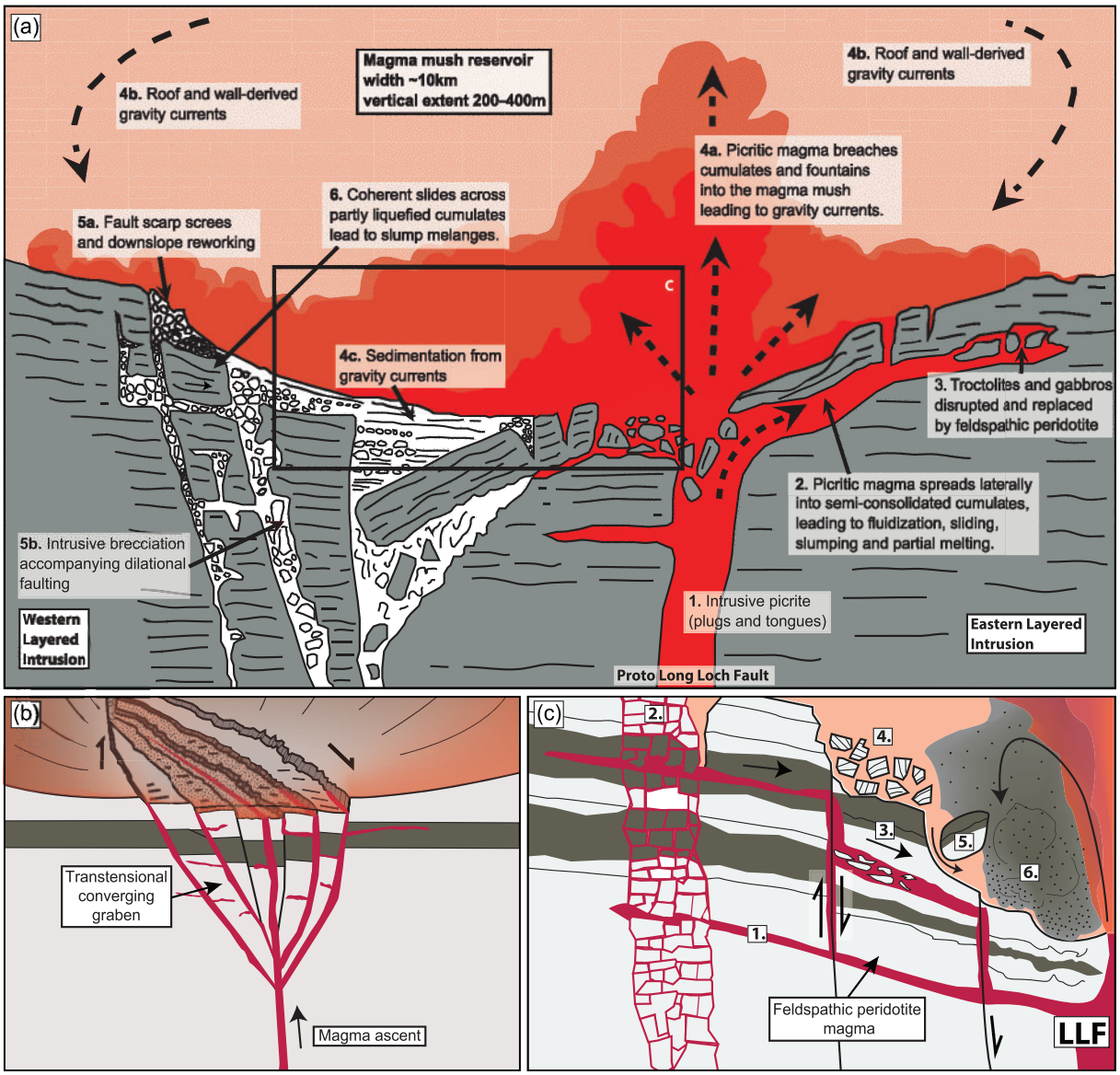

Fig. 18. (a) Periodic replenishments of mafic to picritic magma (1) caused sliding and slumping (2) and intruded laterally into earlier cumulates (3). Magma fountaining into the chamber (4a) probably also caused instability of the roof zone and downward flow of crystal-laden, gravity-driven currents along the sides of the reservoir (4b). Dislodged crystal mushes and reworked loose cumulate debris spread across the floor and were deposited as breccias and dropstones (4c). Faulting and intrusion of feldspathic peridotite, in turn, produced scree breccias (5a) and intrusive brecciation (5b). Slides of larger coherent blocks of cumulate above ductile cumulate mushes led to spectacular slump mélanges (6) (modified after Emeleus *et al.*, 1996). (b) The Long Loch Fault system probably displayed a number of fault splays at the bottom of the shallow reservoir. (c) Conceptual sketch explaining the formation of breccia types in the Central Series. (1) Intrusion of feldspathic peridotite along cumulate bedding and dilating weaknesses in the rock. (2 and 3) Faulting and associated intrusive brecciation separated the cumulate pile into large blocks, and some of them slowly started to slide towards the Long Loch Fault once recharge ceased. As indicated by sheared clasts, these mega-blocks slid along bedding planes where the intruded feldspathic peridotite magma likely acted as a lubricant. (4) Faulting created scarps in the cumulate pile, and the formation of large angular breccias deposited below the scarps. (5) Rotational collapse of detached blocks in-between fault splays in the Long Loch graben led locally to overturned blocks. (6) Reworked clasts (e.g. the 'pebbly' peridotite) were deposited lowest in the magma reservoir. At times of quiescence the suspended cumulate olivines also sedimented in topographical lows in the magma chamber, while subsequent renewed upwelling probably caused repeated re-deposition.

enabled by the hydrous veins and dykelets of feldspathic peridotite and gabbro that formed a dense network in the Central Series by exploiting weaker pathways, such as pre-existing layering and fractures related to the graben-forming transtensional stresses (c.f. McClurg, 1982; Volker, 1983; Butcher *et al.*, 1985; Mattsson, 2014). Fracturing may also have been aided by fluid or vapour exsolution during ascent of the magma that promoted fracture dilation. Additionally, the poikilo-macro-spherulitic feldspar texture is now recognised throughout the Central Series and might occur especially intensely in close association with the veins (Fig. 7e and f). The zonation of the plagioclase interstices in the poikilo-macro spherulites is a possible indication of

relatively evolved plagioclase-rich melt being present or migrating through the Central Series cumulates (Fig. 14a and b). This idea of an evolved liquid is supported by the trace-element pattern of the poikilo-macrospherulite textured peridotites, which are enriched in LREE, especially in La (Fig. 17b) (c.f. Reiners, 1998; Lissenberg *et al.*, 2013).

Furthermore, the 'pebbly' mass-flow-style peridotites are more LREE-enriched than the Central Series peridotites with zoned interstitial minerals (Fig. 17b), which is consistent with the observation that the 'pebbly' peridotite micro-breccia is a mix of older olivine-rich cumulate fragments and a Central Series plagioclase-rich matrix that likely represents an evolved recharge melt. These clasts ('pebbles') were deposited in the deepest part of the Rum reservoir, which was on or close to the magmatic feeder zone (the Long Loch Fault), the site of the most intense recharge injections (Fig. 18).

The harrisite olivines in the feldspathic peridotite of the Central Series were previously considered to represent a supersaturated filter-pressed residual liquid from lower in the cumulate pile which could have brought about reactive liquid flow (see Wadsworth, 1961, 1992, **p. 791**; Donaldson, 1982; Volker & Upton, 1990). Moreover, the komatiitic composition of the feldspathic peridotite dykes and veins indicates that the harrisite crystallization in the Central Series was probably aided by the loss of evolved melt and by fluid exsolution due to decompression on ascent and by replenishing magmas entering a cooler environment at shallower crustal levels (see Figs 13, 17).

Feeding the Rum Layered Suite

While Tait (1985) concluded that magma replenishments at Rum comprised picritic melts from which olivine crystallized, Gibb (1976) held the view that the recharge magmas were highly olivine-phyric (picritic). The question of crystallization in layered intrusions has by now become part of a much wider discussion (Huppert & Sparks, 1981; Marsh, 1996, 2013, 2015; Latypov, 2015) and although crystal-poor replenishing magmas have been considered for Rum by some workers (e.g. Huppert & Sparks, 1981; O'Driscoll *et al.*, 2007*a*), the picrite dykes described, for example, by Upton *et al.* (2002) contain different populations of large olivine and a deeper origin is implied (see also Emeleus *et al.*, 1996; Meyer *et al.*, 2009; Hughes *et al.*, 2016). This is consistent with our analysed pyroxene crystals, which crystallized at between 180 and 650 MPa (6–22 km), and hence significantly below the emplacement level of the current Rum exposures (Fig. 16). Unfortunately, no olivine barometer exists at present, but noteably, deep (mid-crustal) depth of crystallization has recently been determined for clinopyroxene samples of several historical eruptions in Iceland (c.f. Keiding & Sigmarsson 2012; Neave *et al.*, 2019) and we therefore argue that the layered peridotites of the Eastern and Western Layered Series were at least in part assembled through gravitational deposition from crystal-rich recharge magmas. This is in line with the observation that the layered units of the ELS tend to become more olivine-rich closer to the Central Series feeder zone (Volker & Upton, 1990), implying proximal olivine deposition in respect to the Central Series feeder zone, while plagioclase +/-pyroxene may have preferentially been settled at greater distances from the central feeder zone. It may be that each newly arrived low viscosity magma batch, intruded above its compacting predecessor as the latter became depleted of its residual (basaltic) magma. This observation may hint at settling of crystal cargo near the recharge site and also led to new crystallization due to decompression and consequent supersaturation of the replenishing magma in olivine. Floor subsidence may have played a role too at this stage, as indicated by e.g. tilted layers on Trollaval (Volker & Upton, 1990). An analogous, but smaller-scale, demonstration of this phenomenon may be exhibited in the Younger Giant Dyke at Tuttutooq, South Greenland, where the peridotite:troctolite ratio decreases from the intrusion centre to the distal parts (Upton, 2013). Notably, the layered cumulates on Rum became inclined towards the conduit as a result of compaction and likely subsidence (downward collapses). This was aided by creep and slumping of the unconsolidated olivine cumulus, recorded by contorted and slumped layering (e.g. as seen on Trollaval, Volker, 1983; Volker & Upton, 1990).

On Rum, crystal-rich mafic and ultramafic magma, thus, intruded periodically through opening segments of the Long Loch Fault and recharged the shallow Rum magma chamber. Incoming crystals as well as crystals that formed *in situ* then gradually accumulated at the chamber floor until a new larger influx started a new unit (or cycle) of cumulates. For each replenishment, we envisage that resident and some of the recharge magma have likely been expelled to the surface. Waning of each magma influx accompanied collapse of the layered cumulate units and the crystal mush into the graben above the Long Loch Fault (Figs 4, 5, 6).

Considering all the evidence, we suggest that the Central Series operated like a valve-like conduit, undergoing successive dilations and closures that regulated influx of magma into the shallow magma chamber from a deeper reservoir. Indeed, McQuillin & Tuson (1963) suggested on the basis of the large positive Bouguer anomaly that a mafic ultramafic body extends down to ~16 km depth on the basis of a positive Bouguer anomaly over the Layered Series. Remarkably, the average crystallization depth of our Central Series pyroxene crystals is ~16 km (Fig. 16), which provides support that a deeper mid to lower-crustal storage reservoir existed and fed the shallow-level Rum chamber.

The pulsing of magma into the shallow Rum magma reservoir was inferentiallly caused by the magma-induced transtensional tectonic regime of the Long Loch Fault (c.f. Figs 10 and 11), permitting magma ascent during fault movement. The reasons for the

postulated rhythmic fault movements of the Long Loch Fault probably relate to lithospheric stresses acting on the region in Palaeocene times. These influences include the North Atlantic tectonic regime linked to the Iceland plume (c.f. Poore *et al.*, 2009; Lovell, 2010; Horni *et al.*, 2017) and possibly also the interaction of the North Atlantic tectonic regime with far-field tectonic stresses caused by, for example, the Alpine orogeny (e.g. Cooper *et al.*, 2012; Anderson *et al* 2016). This likely resulted in episodic stress release and associated fault activity in the region. The tectono-magmatic evidence presented above also implies that the seismicity of Long Loch Fault controlled magma ascent and triggered down-slope mass-flow of crystal mushes within the Rum magma reservoir (Figs 5 and 6). Such migration of olivine-rich cumulus would have contributed to the dominantly peridotitic nature of the Central Series. When episodic magma influx waned, subsidence and collapse of broken material along the Long Loch Fault would have shut the magma conduit. In between fault movements, magma pressure then built up again in the deeper system, before being released by fault movements and associated conduit opening, during which rapid ascent of primitive, and in part crystal-rich magma was probably promoted. This allowed dense and crystal-rich picrite magmas to ascend (c.f. Upton *et al.*, 2002; Manconi *et al.*, 2009; Allan *et al.*, 2013). The ascending magma would then have spread out laterally on arrival in the shallow Rum chamber, likely in sill-like fashion, which may be the reason for the repeated truncation of growth of some harrisite crystal gardens (see Donaldson, 1975; Gibb, 1976; O'Driscoll *et al.*, 2007*a*, Hepworth *et al.* 2020*b*). Lateral magma movement was terminated by, for example, the Main Ring Fault or by ductile country rocks, as seen in the two marginal zones and at Harris Bay (see Emeleus & Troll, 2008, 2011, 2014). In addition, the liberation of water as magma migrated towards the surface and within the Rum magma system would have produced high fluid contents in the Central Series, assisting fracturing and rock disintegration during replenishment episodes in a style akin to 'magma fracking' (c.f. Boorman *et al.*, 2003). The phenomenon of volatile loss and associated high fluid pressure in the Central Series is probably reflected in the harrisite textures of the feldspathic peridotite veins (Fig. 3), where volatile exsolution and migration from the veins would have raised the liquidus in the system and thus induced rapid crystallization onto existing nucleii (e.g. Sparks & Pinkerton, 1978). Furthermore, within the blocks and matrix of the Central Series, widespread formation of poikilo-macro-spherulitic feldspar textures occurred in many places and is associated with increased deuteric alteration (c.f. Donaldson *et al.*, 1973), implying that hydrous fluids and magmas played a considerable role during their formation and thus during considerable intervals of the lifetime of the Central Series. In addition, intruding feldspathic peridotite would also have partially melted and/or reacted with cumulate layers in the Central Series region (c.f. Leuthold *et al.*, 2014), facilitating slab detachment and collapse towards the feeder zone once recharge pressure subsided (Figs 5 and 6). Widespread slump and shear structures indicate mechanical instability of already solidified cumulate units and crystal mushes (Fig. 6a, c, and d) (c.f. Emeleus, 1997; Emeleus & Troll, 2014).

Building the Rum edifice

The nature of the roof over the Layered Series remains uncertain (Walker, 1975; Donaldson, 1983; Chambers *et al.*, 2005; Troll *et al.*, 2008; Emeleus & Troll, 2014). The present erosion level of the Layered Series lies at shallow plutonic (i.e. sub-volcanic) levels (c.f. Donaldson, 1983; Emeleus, 1997; Troll *et al.*, 2008; Macdonald *et al.*, 2013) and Figs 18 and 19 present a schematic reconstruction of the volcano and its subsurface anatomy that is based on the assumption that most of the layered units crystallized from sheet-like magma bodies. The premises on which Figs 18 and 19 are based are as follows: (1) Erosion and major landslips accompanied episodic diapiric uplift associated with magma emplacement (c.f. Emeleus, 1996, 1997; Troll *et al.*, 2000) and stripped almost all early Palaeocene lavas and Mesozoic strata, plus a great thickness (up to 2 km) of Torridonian strata. Rapid erosion left the lowermost Torridonian and the underlying Lewisian exposed above the magma reservoir at the onset of silicic caldera-style volcanism (Stage 1, Emeleus *et al.*, 1996; Emeleus & Troll, 2011, 2014). (2) Thus, at the onset of Stage 2, the roof overlying the mafic/ultramafic complex comprised some Lewisian and lower Torridonian rocks and some minor downfaulted Jurassic strata and early Palaeocene plateau lavas, plus caldera-fill breccias and silicic extrusive and intrusive rocks (Troll *et al.*, 2000, 2004). (3) Following Brown (1956), crystallization of each layered unit ended with expulsion of residual basalt magma, which eventually generated a basaltic volcano above (Dunham, 1970; Emeleus, 1997; Troll *et al.*, 2008). Dykes within the Eastern and the Western Layered Series are scarce. An explanation for their virtual absence from the layered units may be that magma expulsion was accomplished via dykes from the Central Series that would then have been part of the now eroded volcanic superstructure. Evidence for this basaltic edifice is now preserved in the basaltic clasts in conglomerates interbedded with the Canna lavas in NW Rum (Emeleus, 1985) and in form of meta-basalt (beerbachite) xenoliths in the layered suite (e.g. Emeleus & Troll, 2008). Thus combined with the close spatial, temporal and compositional linkage between the plugs and the Central Series, plus the evidence that the plugs supplied surface activity (Holness *et al.*, 2012), leads us to propose that the Central Series acted as an intermittent magmatic conduit for the Rum intrusion. Inferentially, the faulting recorded in the Central Series and along the Long Loch Fault (Figs 10 and 11), almost inevitably, would have had a surface expression, and we suggest that the overlying volcano

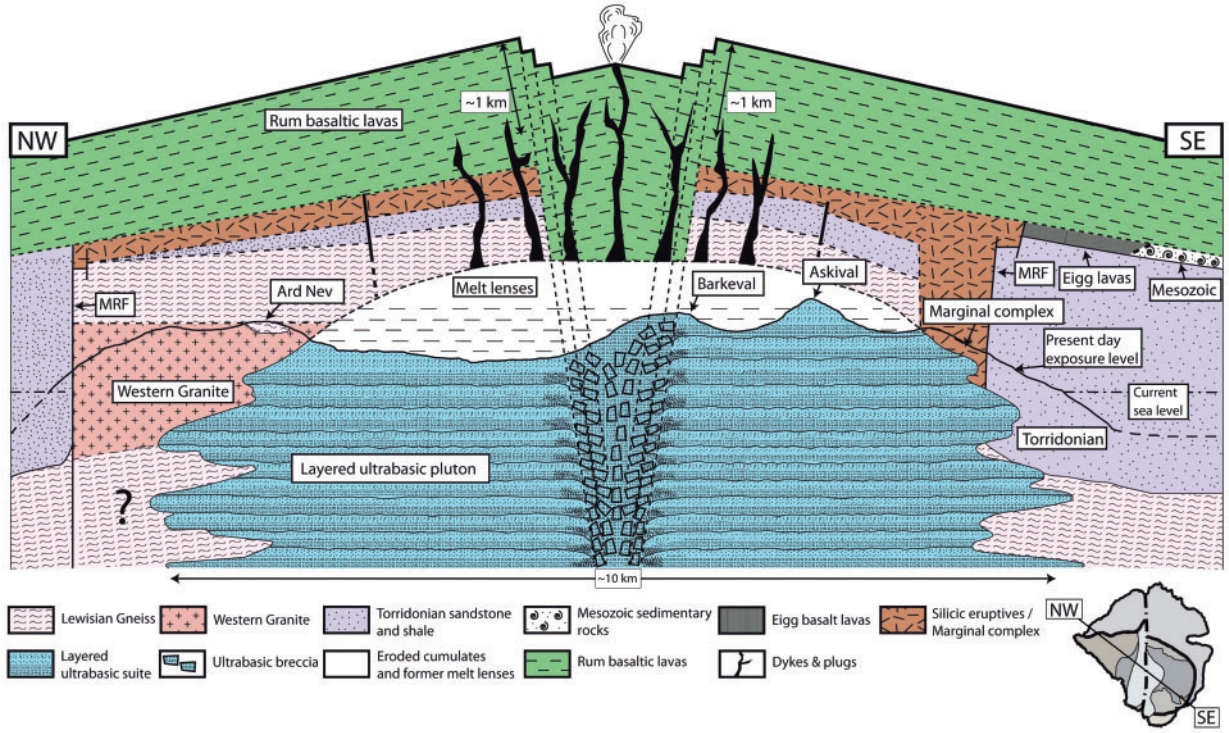

Fig. 19. A schematic reconstruction of the situation envisaged when the mafic–ultramafic complex (the Layered Ultrabasic Suite) was evolving beneath a volcanic carapace. The broad central area between the outward-dipping faults (that experienced dramatic early uplift) contains severely thinned crust. The latter comprises Lewisian gneiss, arenites of the Torridon Group and products of the early silicic volcano ('Marginal Complex'). This rift zone is assumed to persist down to depths of several kilometres and with picritic and basaltic melt lenses on top. Eroded layers are indicated by broken horizontal lines. The axial zone (c.5 km wide) beneath the volcano-graben is distinguished by collapse structures and 'intrusive breccias' and makes up the Central Series. Outside the uplifted area of the former apical dome, the thicker crust comprises early Palaeocene lavas (Eigg Lava Formation), Mesozoic strata, and a much greater thickness of Torridonian arenites above Lewisian gneisses.

could have displayed a volcano-rift system or surface graben (Fig. 19) (Upton, 2004). The erupted lavas probably constructed a low-angled shield- or ridge-type volcanic edifice. The pulsatory nature of magma ascent that generated the Rum Layered Suite would have been reflected in the growth of the overlying volcano, with eruption cycles separated by extended periods of quiescence on perhaps a decadal timescale (e.g. Emeleus & Troll, 2014). Erosional degradation of the volcano may have already taken place during its construction. Evidence from fluvial deposits in western Rum, Canna and northern Skye points to rapid erosion rates that unroofed the Rum Central Complex shortly after its emplacement (Dunham & Emeleus, 1967; Emeleus, 1985; Emeleus & Bell, 2005; Troll *et al.*, 2008).

Summary and concluding remarks

The Rum Igneous Centre, noted amongst the BIPIP volcanoes because of its rhythmic ultrabasic character (Emeleus & Bell, 2005), represents a shallow-crustal magma-holding chamber. Shallow magma storage and heat-loss resulted in large-scale deposition of antecryst and newly formed olivine populations, together with variable amounts of plagioclase (e.g. Brown, 1956; Emeleus *et al.*, 1996). Residual magmas that erupted would probably have been olivine-depleted (low Mg-basalts or hawaiites). The Rum Central Series (e.g. McClurg, 1982), has been relatively neglected by researchers, partly because of its relative inaccessibility but primarily because of its extreme complexity. It however reveals a remarkable testimony to the dynamics within magma reservoirs in active tectonic settings that are periodically replenished over periods of time that may vary from hours to days to thousands of years (c.f. Allan *et al.*, 2013). Coinciding with the Long Loch Fault zone, it provides dramatic evidence of a highly dynamic fault-controlled tectono-magmatic system. Trans-tensional faulting within the Central Series permitted intermittent extraction and ascent of buoyant magma from a deeper crystal mush system to intrude the upper crust and to erupt at its surface. Each eruptive event was succeeded by the draw-back of cooler, crystal-rich residual magmas. Each withdrawal caused fault-drag of ductile side-walls and the collapse of layered rock masses (on all scales), together with olivine-rich slurries. The breccias in the Central Series are attributed to (1) slumping and re-deposition of solidified cumulate materials from the Eastern and Western Layered Series during active periods of the Long Loch Fault, and (2) to disruption of earlier cumulates as well as of

unconsolidated mush by recharging pulses of picritic to evolved basaltic magmas that rose along the Long Loch feeder zone. The floor of the reservoir experienced numerous influxes, ultimately giving rise to a range of breccia-types that include infiltration breccias, slide and rotated breccia blocks, debris-flow breccias, 'conglomeratic' units, and notably enormous raft-like polylithic 'mega-blocks' up to hundreds of metres across that are now embedded within the Central Series breccia mélange. Fault movement and associated earthquakes as well as magma recharge would have induced gravitational collapses of parts of the Rum reservoir and conduit system. Collapse involved normal faulting of mechanically coherent marginal rocks, sagging of still ductile cumulates, and the down-slope avalanching of incoherent crystal-liquid mushes and large slabs of variously solidified cumulate materials. The widespread feldspathic peridotite veins in the Central Series record simultaneous intrusive activity and melt migration, as do the many gabbro and peridotite plugs. Therefore, a combination of repeated injections and associated structural collapses can account for the formation of the Central Series (Figs 18 and 19). We envisage that movements along the Long Loch Fault were episodic and occurred when accumulated extensional strain exceeded the strength of the local country-rock. Pulses of primitive to evolved hydrous basaltic magmas moved through the Long Loch Fault feeder system, probably controlled by fault movements and likely separated by times of inactivity. This would have allowed pressure to build up and differentiation to more evolved basaltic magmas with relatively higher H_2O contents in the deeper (mid- to lower-crustal) magma plumbing system. Major fault movements would then have allowed volatile-rich and at times crystal-rich magmas to rapidly ascend into the shallow-level Rum magma reservoir where much of the crystal cargo was ultimately deposited. This post-eruptive aftermath left an exceedingly chaotic mélange now exposed in the hearth of the early Palaeocene Rum volcano. Ascent of primitive high-magnesium and transitionally alkaline basalt magmas that were fed laterally into shallow-crustal sill-like intrusions to either side of the this active fault zone are now seen in the more ordered sequences of the Eastern and Western Layered Series and may be thought of as the essentially undisturbed parts of the chamber. The Long Loch Fault was therefore critical in placing geological control on the location of the Rum volcano and for creating a channelway for the rhythmically layered character of its Layered Suite as well as for the chaotically disrupted materials composing the Central Series.

ACKNOWLEDGEMENTS

We dedicate this article to the memory of Charles Henry Emeleus (September 4, 1930 – November 11, 2017), who over six decades, contributed much to mapping and understanding of the geology and petrology of Rum, to mentoring the many undergraduate and doctoral students who have worked there, and to promoting public interest in its geological history. He will be missed dearly. Our understanding of the geology of Rum and the Central Series has also profited greatly from discussions with J. Bédard, S. Burchardt, A. Butcher, G. P. Black, M H. P. Bott, G. M. Brown, M. Cheadle, J. Davidson, A. C. Dunham, J. Faithfull, M. Forster, A. Fowler, K. Goodenough, R. Greenwood, L. Hepworth, E.P. Holohan, M. Holness, R. H. Hunter, J. Leuthold, D. Jerram, D. Kitchen, J. McClurg, F. C. Meade, I. Meighan, G.R. Nicoll, P. J. Nicholson, B. O'Driscoll, R. Renner, R. Sides, M. Smith, S. R. Tait, F. J. Tepley, J. Volker, J. Wadsworth and I. M. Young. The authors are also grateful for field work and logistical support by J. Volker, J. McClurg, G.R. Nicoll, E.P. Holohan and S. Burchardt, and for help with figure drafting from K. Thomaidis and H. Geiger. The authors are also grateful to J. Gamble, R. Latypov and D. Jerram for constructive journal reviews and to M. Wilson and T. E. Waight for the editorial handling of the manuscript. Our work on Rum has been made possible through the help and encouragement of the past and present scientific and estate staff of the Nature Conservancy Council and Scottish Natural Heritage, on and off the island. The authors acknowledge the use of the Move SoftwareSuite granted by Midland Valley's Academic Software Initiative/Petroleum Experts.

FUNDING

Financial support by the Swedish Science Foundation (Vetenskapsrådet), Uppsala University, and the Clough Fund of the Geological Society of Edinburgh are gratefully acknowledged.

SUPPLEMENTARY DATA

Supplementary data are available at *Journal of Petrology* online

REFERENCES

Á Horni, J., Hopper, J., Blischke, A., Geisler, W., Stewart, M., McDermott, K., Judge, M., Elendsson, Ö. & Arting, U. (2017). *Regional Distribution of Volcanism within the North Atlantic Igneous Province*. Geological Society of London Special Publications **447**: 105–125.

Allan, A. S. R., Morgan, D. J., Wilson, C. J. N. & Millet, M.-A. (2013). From mush to eruption in centuries: assembly of the super-sized Oruanui magma body. *Contributions to Mineralogy and Petrology* **166**, 143–164.

Allan, A. S. R., Wilson, C. J. N., Millet, M.-A. & Wysoczanski, R. J. (2012). The invisible hand: Tectonic triggering and modulation of a rhyolitic supereruption. *Geology* **40**, 563–566.

Anderson, H., Walsh, J. & Cooper, M. (2016). Faults, intrusions and Flood Basalts: The Cenozoic structure of the North of Ireland. In: Young M. (ed.) *Unearthed: Impact of the Tellus Surveys of the North of Ireland*. Dublin, Ireland: Royal Irish Academy, pp. 179–189.

Bailey, E. B., Clough, C. T., Wright, W. B., Richey, J. E. & Wilson, G. V. (1924). *The Tertiary and Post-Tertiary Geology of Mull, Loch Aline and Oban*. Edinburgh, UK: Memoir of the Geological Survey of Great Britain, Sheet 44 (Scotland), HMSO.

Barker, A. K., Troll, V. R., Carracedo, J. C. & Nicholls, P. A. (2015). The magma plumbing system for the 1971 Teneguía eruption on La Palma, Canary Islands. *Contributions to Mineralogy and Petrology* **170**, 54.

Beard, J. S., Ragland, P. C. & Rushmer, T. (2004). Hydration crystallization reactions between anhydrous minerals and hydrous melt to yield amphibole and biotite in igneous rocks: Description and implications. *The Journal of Geology* **112**, 617–621.

Bédard, J. H., Sparks, R. S. J., Renner, R., Cheadle, M. J. & Hallworth, M. A. (1988). Peridotite sills and metasomatic gabbros in the Eastern Layered Series of the Rhum complex. *Journal of the Geological Society* **145**, 207–224.

Bell, B. R. & Williamson, I. T. (2002). Tertiary Igneous activity. In: Trewin, N. H. (ed.) *The Geology of Scotland.* UK: The Geological Society London, pp. 371–407.

Beran, A. (1976). Messung des Ultrarot-Pleochroismus von Mineralen. XIV. Der Pleochroismus der OH-Streckfrequenz in Diopsid. *TMPM Tschermaks Mineralogische und Petrographische Mitteilungen* **23**, 79–85.

Boorman, S. L., McGuire, J. B., Boudreau, A. E. & Kruger, J. F. (2003). Fluid overpressure in layered intrusions: formation of a breccia pipe in the Eastern Bushveld Complex, Republic of South Africa. *Mineralium Deposita* **38**, 356–369.

Brown, G. M. (1956). The Layered Ultrabasic Rocks of Rhum, Inner Hebrides. *Philosophical Transactions of the Royal Society of London B: Biological Sciences* **240**, 1–54. [10.1098/rstb.1956.0011]

Butcher, A. R. (1985). Channelled metasomatism in Rhum layered cumulates – evidence from late-stage veins. *Geological Magazine* **122**, 503–518.

Butcher, A. R., Young, I. M. & Faithfull, J. W. (1985). Finger structures in the Rhum Complex. *Geological Magazine* **122**, 491–502.

Cashman, K., Sparks, R. S. J. & Blundy, J. D. (2017). Vertically extensive and unstable magmatic systems: a unified view of igneous processes. *Science* **355**, eaag3055. eaag

Chambers, L. M., Pringle, M. S. & Parrish, R. R. (2005). Rapid formation of the Small Isles Tertiary centre constrained by precise $^{40}Ar/^{39}Ar$ and U–Pb ages. *Lithos* **79**, 367–384.

Cooper, M. R., Anderson, H., Walsh, J. J., Van Dam, C. L., Young, M. E., Earls, G. & Walker, A. (2012). Palaeogene Alpine tectonics and Icelandic plume-related magmatism and deformation in Northern Ireland. *Journal of the Geological Society* **169**, 29–36.

D'Oriano, C., Pompilio, M., Bertagnini, A., Cioni, R. & Pichavant, M. (2013). Effects of experimental reheating of natural basaltic ash at different temperatures and redox conditions. *Contributions to Mineralogy and Petrology* **165**, 863–883.

Donaldson, C. H. (1974). Olivine crystal types in Harrisitic rocks of the Rhum Pluton and in Archean spinifex rocks. *Geological Society of American Bulletin* **85**, 1721–1726.

Donaldson, C. H. (1975). Ultrabasic Breccias in layered intrusions: The Rhum Complex. *The Journal of Geology* **83**, 33–45. [https://www.jstor.org/stable/30062337]

Donaldson, C. H. (1976). An experimental investigation of olivine morphology. *Contributions to Mineralogy and Petrology* **57**, 187–213.

Donaldson, C. H. (1982). Origin of some of the Rhum Harrisite by segregation of intercumulus liquid. *Mineralogical Magazine* **45**, 201–209.

Donaldson, C. H. (1983). Tertiary igneous activity in the Inner Hebrides. *Proceedings of the Royal Society of Edinburgh Section B Biological Sciences* **83**, 65–81.

Donaldson, C. H., Drever, H. I. & Johnston, R. (1973). Crystallization of Poikilo-macro-spherulitic Feldspar in a Rhum Peridotite. *Nature Physical Science* **243**, 69–70.

Donaldson, C. H., Troll, V. R. & Emeleus, C. H. (2001). Felsites and breccias in the Northern Marginal Zone of the Rum Central Complex: changing views, c. 1900-2000. *Proceedings of the Yorkshire Geological Society* **53**, 167–175.

Dunham, A. C. (1970). The emplacement of the Tertiary igneous complex of Rhum. *Geological Journal, Special Issue No. 2,* 23–32.

Dunham, A. C. & Emeleus, C. H. (1967). The Tertiary Geology of Rhum, Inner Hebrides. *Proceedings of the Geologists' Association* **78**, 391–418.

Dunham, A. C. & Wadsworth, W. J. (1978). Cryptic variation in the Rhum layered intrusion. *Mineralogical Magazine* **42**, 347–356.

Ejima, T., Akasaka, M., Nagao, T. & Ohfuji, H. (2015). Occurrence of Fe^{3+} and formation process of precipitates within oxidized olivine phenocrysts in basalt lava from Kuroshima volcano, Goto Islands, Nagasaki, Japan. *Mineralogical Magazine* **79**, 1833–1848.

Emeleus, C. H. (1985). The Tertiary lavas and sediments of northwest Rhum, Inner Hebrides. *Geological Magazine* **122**, 419–437.

Emeleus, C. H. (1997). *Geology of Rum and the Adjacent Islands. Memoir of the British Geological Survey (Scotland)*. London: The Stationary Office.

Emeleus, C. H. (2004). *Rum solid geology map 1:20000*.

Emeleus, C. H. & Bell, B. R. (2005). *British Regional Geology: The Palaeogene Volcanic Districts of Scotland*. Nottingham, UK: British Geological Survey.

Emeleus, C. H., Cheadle, M. J., Hunter, R. H., Upton, B. G. J. & Wadsworth, W. J. (1996). The Rum Layered Suite. In: Cawthorn, R. G. (ed.) *Developments in Petrology*. Amsterdam: Elsevier, pp. 403–439.

Emeleus, C. H. & Troll, V. R. (2008). A Geological Excursion Guide to Rum. *The Paleocene Igneous Rocks of the Isle of Rum, Inner Hebrides*. Edinburgh, UK: Edinburgh Geological Society and the National Museums Scotland, pp. 1–150.

Emeleus, C. H. & Troll, V. R. (2011). Recent research developments on the Isle of Rum, NW Scotland. *Geology Today* **27**, 184–193.

Emeleus, C. H. & Troll, V. R. (2014). The Rum Igneous Centre. *Mineralogical Magazine* **78**, 805–839.

England, R. W. (1988). The early Tertiary stress regime in NW Britain: evidence from the patterns of volcanic activity. *Geological Society, London, Special Publications* **39**, 381–389.

Gamble, J. A. (1979). Some relationships between coexisting granitic and basaltic magmas and the genesis of hybrid rocks in the Tertiary central complex of Slieve Gullion, northeast Ireland. *Journal of Volcanology and Geothermal Research* **5**, 297–316.

Gibb, F. G. F. (1976). Ultrabasic rocks of Rhum and Skye: the nature of the parent magma. *Journal of the Geological Society* **132**, 209–222.

Gillis, K. M., Snow, J. E., Klaus, A., Abe, N., Adrião, Á. B., Akizawa, N., Ceuleneer, G., Cheadle, M. J., Faak, K., Falloon, T. J., Friedman, S. A., Godard, M., Guerin, G., Harigane, Y., Horst, A. J., Hoshide, T., Ildefonse, B., Jean, M. M., John, B. E., Koepke, J., Machi, S., Maeda, J., Marks, N. E., McCaig, A. M., Meyer, R., Morris, A., Nozaka, T., Python, M., Saha, A. &

Wintsch, R. P. (2014a). Primitive layered gabbros from fast-spreading lower oceanic crust. *Nature* **505**, 204–207.

Gillis, K. M., Snow, J. E., Klaus, A., Abe, N., Adrião, Á. B., Akizawa, N., Ceuleneer, G., Cheadle, M. J., Faak, K., Falloon, T. J., Friedman, S. A., Godard, M., Guerin, G., Harigane, Y., Horst, A. J., Hoshide, T., Ildefonse, B., Jean, M. M., John, B. E., Koepke, J., Machi, S., Maeda, J., Marks, N. E., McCaig, A. M., Meyer, R., Morris, A., Nozaka, T., Python, M., Saha, A. & Wintsch, R. P. (2014b). Geochemistry summary. *Proceedings of the Integrated Ocean Drilling Program, Volume* **345**. [10.2204/iodp.proc.345.114.2014]

Girard, G. & van Wyk de Vries, B. (2005). The Managua Graben and Las Sierras-Masaya volcanic complex (Nicaragua); pull-apart localization by an intrusive complex: results from analogue modeling. *Journal of Volcanology and Geothermal Research* **144**, 37–57.

Greenwood, R. C., Donaldson, C. H. & Emeleus, C. H. (1990). The contact zone of the Rhum ultrabasic intrusion: evidence of peridotite formation from magnesian magmas. *Journal of the Geological Society* **147**, 209–212.

Greenwood, R. C., Fallick, A. E. & Donaldson, C. H. (1992). Oxygen isotope evidence for major fluid flow along the contact zone of the Rum ultrabasic intrusion. *Geological Magazine* **129**, 243–246.

Haggerty, S. E. & Baker, I. (1967). The alteration of olivine in basaltic and associated lavas. *Contributions to Mineralogy and Petrology* **16**, 233–257.

Hamilton, M. A., Pearson, D. G., Thompson, R. N., Kelley, S. P. & Emeleus, C. H. (1998). Rapid eruption of Skye lavas inferred from precise U-Pb and Ar-Ar dating of the Rum and Cuillin plutonic complexes. *Nature* **394**, 260–263.

Harker, A. (1908). *The Geology of the Small Isles of Inverness-Shire: (Rum, Canna, Eigg, Muck, Etc.)(Sheet 60, Scotland)*. Glasgow, Scotland. Printed for HMSO, by J. Hedderwick & Sons, Ltd, Memoirs of the Geological Survey.

Hemond, C., Condomines, M., Fourcade, S., Allègre, C. J., Oskarsson, N. & Javoy, M. (1988). Thorium, strontium and oxygen isotopic geochemistry in recent tholeiites from Iceland: crustal influence on mantle-derived magmas. *Earth and Planetary Science Letters* **87**, 273–285.

Hepworth, L. N., Daly, J. S., Gertisser, R., Johnson, C. G., Emeleus, C. H. & O'Driscoll, B. (2020a). Rapid crystallization of precious metal-mineralized layers in mafic magmatic systems. *Nature Geoscience* **13**, 375–381.

Hepworth, L. N., Kaufmann, F. E. D., Hecht, L., Gertisser, R. & O'Driscoll, B. (2020b). Braided pridotite sills and metasomatism in the Rum Layered Suite. *Contributions to Mineralogy and Petrology* **175**, 17.

Hepworth, L. N., O'Driscoll, B., Gertisser, R., Daly, J. S. & Emeleus, C. H. (2017). Incremental Construction of the unit 10 Peridotite, Rum Eastern Layered Intrusion, NW Scotland. *Journal of Petrology* **58**, 137–166.

Higgins, M. D. (2002). Closure in crystal size distributions (CSD), verification of CSD calculations, and the significance of CSD fans. *American Mineralogist* **87**, 171–175. [10.2138/am-2002-0118]

Higgins, M. D. (2000). Measurement of crystal size distributions. *American Mineralogist* **85**, 1105–1116.

Hodgson, J. & Young, M. (2016). The Tellus airborne geophysical surveys and results. In: Young M. (ed.) *Unearthed: Impact of the Tellus Surveys of the North of Ireland*. Dublin, Ireland: Royal Irish Academy, pp. 11–31.

Holness, M. B. (1999). Contact metamorphism and anatexis of Torridonian arkose by minor intrusions of the Rum Igneous Complex, Inner Hebrides, Scotland. *Geological Magazine* **136**, 527–542.

Holness, M. B. (2005). Spatial constraints on magma chamber replenishment events from textural observations of cumulates: The Rum Layered Intrusion, Scotland. *Journal of Petrology* **46**, 1585–1601.

Holness, M. B. (2007). Textural immaturity of cumulates as an indicator of magma chamber processes: infiltration and crystal accumulation in the Rum Eastern Layered Intrusion. *Journal of the Geological Society* **164**, 529–539.

Holness, M. B., Hallworth, M. A., Woods, A. & Sides, R. E. (2007). Infiltration metasomatism of cumulates by intrusive magma replenishment: the Wavy Horizon, Isle of Rum, Scotland. *Journal of Petrology* **48**, 563–587.

Holness, M. B. & Isherwood, C. E. (2003). The aureole of the Rum Tertiary Igneous Complex, Scotland. *Journal of the Geological Society* **160**, 15–27.

Holness, M. B., Sides, R., Prior, D. J., Cheadle, M. J. & Upton, B. G. J. (2012). The peridotite plugs of Rum: Crystal settling and fabric development in magma conduits. *Lithos* **134–135**, 23–40.

Holness, M. B. & Winpenny, B. (2009). The Unit 12 allivalite, Eastern Layered Intrusion, Isle of Rum: a textural and geochemical study of an open-system magma chamber. *Geological Magazine* **146**, 437–450.

Holohan, E. P., van Wyk de Vries, B. & Troll, V. R. (2008). Analogue models of caldera collapse in strike-slip tectonic regimes. *Bulletin of Volcanology* **70**, 773–796.

Hopper, J. R., Funck, T., Stoker, M., Arting, U., Peron-Prinvidic, G., Doornebal, J. C. & Gaina, C. (2014). *Tectonostratigraphic Atlas of the North-East Atlantic Region*. Copenhagen, Denmark: Geological Survey of Denmark and Greenland.

Hughes, H. S. R., McDonald, I., Boyce, A. J., Holwell, D. A. & Kerr, A. C. (2016). Sulphide sinking in Magma conduits: evidence from Mafic-Ultramafic Plugs on Rum and the Wider North Atlantic Igneous Province. *Journal of Petrology* **57**, 383–416.

Huppert, H. E. & Sparks, R. S. J. (1981). The fluid dynamics of a basaltic magma chamber replenished by influx of hot, dense ultrabasic magma. *Contributions to Mineralogy and Petrology* **75**, 279–289.

Irvine, T. N. (1980). Magmatic infiltration metasomatism, double-diffusive fractional crystallization, and adcumulus growth in the muskox intrusion and other layered intrusions. In: Hargraves, R. B. (ed.) *Physics of Magmatic Processes*. Princeton, NJ: Princeton University Press, pp. 325–383.

Irvine, T. N., Andersen, J. C. Ø. & Brooks, C. K. (1998). Included blocks (and blocks within blocks) in the Skaergaard intrusion: Geologic relations and the origins of rhythmic modally graded layers. *Geological Society of America Bulletin* **110**, 1398.

Jamtveit, B., Brooker, R., Brooks, K., Larsen, L. M. & Pedersen, T. (2001). The water content of olivines from the North Atlantic Volcanic Province. *Earth and Planetary Science Letters* **186**, 401–415.

Jolly, R. J. H. & Sanderson, D. J. (1995). Variation in the form and distribution of dykes in the Mull swarm, Scotland. *Journal of Structural Geology* **17**, 1543–1557.

Keiding, J. K. & Sigmarsson, O. (2012). Geothermobarometry of the 2010 Eyafallajökull eruption: new constraints on Icelandic magma plumbing systems. *Journal of Geophysical Research, Solid Earth* **117**, B00C09.

Kerr, A. C., Kent, R. W., Thomson, B. A., Seedhouse, J. K. & Donaldson, C. H. (1999). Geochemical evolution of the Tertiary Mull Volcano, Western Scotland. *Journal of Petrology* **40**, 873–908.

Kitchen, D. E. (1985). The parental magma on Rhum: evidence from alkaline segregations and veins in the peridotites from Salisbury's Dam. *Geological Magazine* **122**, 529–537.

Kovalenko, V. I., Naumov, V. B., Girnis, A V., Dorofeeva, V. A. & Yarmolyuk, V. V. (2007). Volatiles in basaltic magmas of ocean islands and their mantle sources: I. Melt compositions deduced from melt inclusions and glasses in the rocks. *Geochemistry International* **45**, 105–122.

Latypov, R. (2015). A fundamental dispute: a discussion of "On some fundamentals of Igneous Petrology" by Bruce D. Marsh, Contributions to Mineralogy and Petrology (2013) **166**: 665–690. *Contributions to Mineralogy and Petrology* **169**, 20. [10.1007/s00410-015-1108-9}

Lawver, L. A. & Muller, R. D. (1994). Iceland hotspot track. *Geology* **22**, 311–314.

Le Bas, M. J. (1971). Per-alkaline Volcanism, Crustal Swelling, and Rifting. *Nature Physical Science* **230**, 85–87.

Le Bas, M. J. (2000). IUGS reclassification of the high-Mg and Picritic Volcanic Rocks. *Journal of Petrology* **41**, 1467–1470.

Leuthold, J., Blundy, J. D. & Brooker, R. A. (2015). Experimental Petrology Constraints on the Recycling of Mafic Cumulate: A Focus on Cr-Spinel from the Rum Eastern Layered Intrusion, Scotland. *Contributions to Mineralogy and Petrology*. **170**, 1–27.

Leuthold, J., Blundy, J. D., Holness, M. B. & Sides, R. (2014). Successive episodes of reactive liquid flow through a layered intrusion (Unit 9, Rum Eastern Layered Intrusion, Scotland). *Contributions to Mineralogy and Petrology* **168**, 1021.

Libowitzky, E. & Rossman, G. R. (1997). An IR absorption calibration for water in minerals. *American Mineralogist* **82**, 1111–1115.

Lissenberg, C. J., MacLeod, C. J., Howard, K. A. & Godard, M. (2013). Pervasive reactive melt migration through fast-spreading lower oceanic crust (Hess Deep, equatorial Pacific Ocean). *Earth and Planetary Science Letters* **361**, 436–447.

Lovell, B. (2010). A pulse in the planet: regional control of high-frequency changes in relative sea level by mantle convection. *Journal of the Geological Society* **167**, 637–648.

Macdonald, R., Bagiński, B., Dzierżanowski, P. & Jokubauskas, P. (2013). Apatite-supergroup minerals in UK Palaeogene granites: composition and relationship to host-rock composition. *European Journal of Mineralogy* **25**, 461–471.

Macdonald, R., Bagiński, B., Upton, B. G. J., Dzierżanowski, P., Marshall-Roberts, W. & Prieto, M. (2009). The Palaeogene Eskdalemuir dyke, Scotland: long-distance lateral transport of rhyolitic magma in a mixed-magma intrusion. *Mineralogical Magazine* **73**, 285–300.

Macdonald, R., Fettes, D. J. & Bagiński, B. (2015). The Mull Paleocene dykes: some insights into the nature of major dyke swarms. *Scottish Journal of Geology* **51**, 116–124.

Manconi, A., Longpre, M.-A., Walter, T. R., Troll, V. R. & Hansteen, T. H. (2009). The effects of flank collapses on volcano plumbing systems. *Geology* **37**, 1099–1102.

Marsh, B. (2015). Reply. *Contributions to Mineralogy and Petrology* **169**, 21.

Marsh, B. D. (1981). On the crystallinity, probability of occurrence, and rheology of lava and magma. *Contributions to Mineralogy and Petrology* **78**, 85–98.

Marsh, B. D. (1996). Solidification fronts and magmatic evolution. *Mineralogical Magazine* **60**, 5–40.

Marsh, B. D. (2013). On some fundamentals of igneous petrology. *Contributions to Mineralogy and Petrology* **166**, 665–690.

Mathieu, L. & van Wyk de Vries, B. (2011). The impact of strike-slip, transtensional and transpressional fault zones on volcanoes. Part 1: Scaled experiments. *Journal of Structural Geology* **33**, 907–917.

Mathieu, L., van Wyk de Vries, B., Pilato, M. & Troll, V. R. (2011). The interaction between volcanoes and strike-slip, transtensional and transpressional fault zones: analogue models and natural examples. *Journal of Structural Geology* **33**, 898–906.

Mattsson, T. (2014). The Roots of a Magma Chamber, the Central Intrusion, Rum, NW-Scotland. In: *Examensarbete Vid Institutionen För Geovetenskaper NV - 304*. Department of Earth Sciences, Earth Sciences, Disciplinary Domain of Science and Technology, Master thesis, Uppsala University.

McClurg, J. E. (1982). Petrology and evolution of the northern part of the Rhum ultramafic complex. Ph.D. thesis, University of Edinburgh.

McDonough, W. F. & Sun, S. S. (1995). The composition of the Earth. *Chemical Geology* **120**, 223–253.

McQuillin, R. & Tuson, J. (1963). Gravity Measurements over the Rhum Tertiary Plutonic Complex. *Nature* **199**, 1276–1277.

Meade, F. C., Troll, V. R., Ellam, R. M., Freda, C., Font, L., Donaldson, C. H. & Klonowska, I. (2014). Bimodal magmatism produced by progressively inhibited crustal assimilation. *Nature Communications*. Nature Publishing Group **5**, 1–11.

Meyer, R., Nicoll, G. R., Hertogen, J. G. H., Troll, V. R., Ellam, R. M. & Emeleus, C. H. (2009). Trace element and isotope constraints on crustal anatexis by upwelling mantle melts in the North Atlantic Igneous Province: an example from the Isle of Rum, NW Scotland. *Geological Magazine* **146**, 382–399.

Meyer, R. & van Wijk, J. (2015). Post-breakup lithosphere recycling below the U.S. East Coast: Evidence from adakitic rocks. Geological Society of America Special Paper **514**, 65–85.

Meyer, R., van Wijk, J. & Gernigon, L. (2007). The North Atlantic Igneous Province: a review of models for its formation. In: Foulger, G. R., & Jurdy, D. M. (eds) *Plates, Plumes and Planetary Processes*. Geological Society of America Special Paper 430, [10.1130/SPE430]

Morimoto, N. (1988). Nomenclature of pyroxenes. *Mineralogy and Petrology* **39**, 55–76.

Nazzareni, S., Skogby, H. & Zanazzi, P. F. (2011). Hydrogen content in clinopyroxene phenocrysts from Salina mafic lavas (Aeolian arc, Italy). *Contributions to Mineralogy and Petrology* **162**, 275–288.

Neave, D., Bali, E., Gudfinnsson, G. H., Halldorsson, S., Kahl, M., Schmidt, A.-S. & Holtz, F. (2019). Clinopyroxene-liquid equilibria and geothermobarometry in natural and experimental tholeiites: the 2014-2015 Holuhraun eruption, Iceland. *Journal of Petrology* **60**, 1653–1680.

Nichols, A. R. L., Carroll, M. R. & Höskuldsson, Á. (2002). Is the Iceland hot spot also wet? Evidence from the water contents of undegassed submarine and subglacial pillow basalts. *Earth and Planetary Science Letters* **202**, 77–87.

Nicoll, G. R., Holness, M. B., Troll, V. R., Donaldson, C. H., Holohan, E. P., Emeleus, C. H. & Chew, D. M. (2009). Early mafic magmatism and crustal anatexis on the Isle of Rum: evidence from the Am Màm intrusion breccia. *Geological Magazine* **146**, 368–381.

Nimis, P. (1995). A clinopyroxene geobarometer for basaltic systems based on crystal-structure modeling. *Contributions to Mineralogy and Petrology* **121**, 115–125.

Nozaka, T., Wintsch, R. P. & Meyer, R. (2017). Serpentinization of olivine in troctolites and olivine gabbros from the Hess Deep Rift. *Lithos* **282–283**, 201–214.

O'Driscoll, B., Donaldson, C. H., Daly, J. S. & Emeleus, C. H. (2009). The roles of melt infiltration and cumulate assimilation in the formation of anorthosite and a Cr-spinel seam in the Rum Eastern Layered Intrusion, NW Scotland. *Lithos* **111**, 6–20.

O'Driscoll, B., Donaldson, C. H., Troll, V. R., Jerram, D. A. & Emeleus, C. H. (2007a). An Origin for Harrisitic and Granular

Olivine in the Rum Layered Suite, NW Scotland: a Crystal Size Distribution Study. *Journal of Petrology* **48**, 253–270.

O'Driscoll, B., Emeleus, C. H., Donaldson, C. H. & Daly, J. S. (2010). Cr-spinel seam petrogenesis in the Rum layered suite, NW Scotland: Cumulate assimilation and in situ crystallization in a deforming crystal mush. *Journal of Petrology* **51**, 1171–1201.

O'Driscoll, B., Hargraves, R. B., Emeleus, C. H., Troll, V. R., Donaldson, C. H. & Reavy, R. J. (2007b). Magmatic lineations inferred from anisotropy of magnetic susceptibility fabrics in Units 8, 9, and 10 of the Rum Eastern Layered Series, NW Scotland. *Lithos* **98**, 27–44.

O'Leary, J. A., Gaetani, G. A. & Hauri, E. H. (2010). The effect of tetrahedral Al3+ on the partitioning of water between clinopyroxene and silicate melt. *Earth and Planetary Science Letters* **297**, 111–120.

Okumura, S. (2011). The H2O content of andesitic magmas from three volcanoes in Japan, inferred from the infrared analysis of clinopyroxene. *European Journal of Mineralogy* **23**, 771–778.

Park, R. G., Stewart, A. D. & Wright, D. T. (2002). The Hebridean Terrane. In: Trewin, N. H. (ed.) *The Geology of Scotland*. London: The Geological Society.

Petronis, M. S., O'Driscoll, B., Troll, V. R., Emeleus, C. H. & Geissman, J. W. (2009). Palaeomagnetic and anisotropy of magnetic susceptibility data bearing on the emplacement of the Western Granite, Isle of Rum, NW Scotland. *Geological Magazine* **146**, 419–436.

Poore, H. R., White, N. & Jones, S. (2009). A Neogene chronology of Iceland plume activity from V-shaped ridges. *Earth and Planetary Science Letters* **283**, 1–13.

Preston, J. (2009). "Tertiary Igneous activity. In: Holland, C. H. & Saundes, I. S. (eds) *The Geology of Ireland*. Edinburgh: Dunedin Academic Press, pp. 333–354.

Putirka, K. D. (2008). Thermometers and Barometers for Volcanic Systems. *Reviews in Mineralogy and Geochemistry* **69**, 61–120.

Reiners, P. W. (1998). Reactive melt transport in the mantle and geochemical signatures of mantle-derived magmas. *Journal of Petrology* **39**, 1039–1061.

Renner, R. & Palacz, Z. (1987). Basaltic replenishment of the Rhum magma chamber: evidence from unit 14. *Journal of the Geological Society* **144**, 961–970.

Richey, J. E. (1961). *British Regional Geology: The Tertiary Volcanic Districts of Scotland*. Edinburgh: HMSO for the British Geological Survey.

Saunders, A. D., Fitton, J. G., Kerr, A. C., Norry, M. J. & Kent, R. W. (1997). "The North Atlantic Igneous Province. In: Mahoney, J. J. & Coffin, M. F. (eds) *Large Igneous Provinces: Continental, Oceanic, and Planetary Flood Volcanism*. Washington, DC: American Geophysical Union, pp. 45–93.

Schneider, C. A., Rasband, W. S. & Eliceiri, K. W. (2012). NIH Image to ImageJ: 25 years of image analysis. *Nature Methods* **9**, 671–675.

Skogby, H. (2006). Water in Natural Mantle Minerals I: Pyroxenes. *Reviews in Mineralogy and Geochemistry* **62**, 155–167.

Smith, K. (2012). The Fascadale Fault: A tectonic link between the Cenozoic volcanic centres of Rum and Ardnamurchan, Scotland, revealed by multibeam survey. *Scottish Journal of Geology* **48**, 91–102.

Sparks, R. S. J. & Pinkerton, H. (1978). Effect of degassing on rheology of basaltic lava. *Nature* **276**, 385–386.

Sun, S.-S. & McDonough, W. F. (1989). Chemical and isotopic systematics of oceanic basalts: implications for mantle composition and processes. *Geological Society*, London, Special Publications **42**, 313–345.[10.1144/GSL.SP.1989.042.01.19]

Tait, S. R. (1985). Fluid dynamic and geochemical evolution of cyclic unit 10, Rhum, Eastern Layered Series. *Geological Magazine* **122**, 469–484.

Trippanera, D., Ruch, J., Acocella, V., Thordarson, T. & Urbani, S. (2018). Interaction between central volcanoes and regional tectonics along divergent plate boundaries: Askja, Iceland. *Bulletin of Volcanology* **80**, 1. [10.1007/s00445-017-1179-8]

Troll, V. R., Donaldson, C. H. & Emeleus, C. H. (2004). Pre-eruptive magma mixing in ash-flow deposits of the Tertiary Rum Igneous Centre, Scotland. *Contributions to Mineralogy and Petrology* **147**, 722–739.

Troll, V. R., Emeleus, C. H. & Donaldson, C. H. (2000). Caldera formation in the Rum Central Igneous Complex, Scotland. *Bulletin of Volcanology* **62**, 301–317.

Troll, V. R., Nicoll, G. R., Donaldson, C. H. & Emeleus, C. H. (2008). Dating the onset of volcanism at the Rum Igneous Centre, NW Scotland. *Journal of the Geological Society* **165**, 651–659.

Upton, B. G. J. (2004). *Volcanoes and the Making of Scotland*. Edinburgh, UK: Dunedin Academic Press.

Upton, B. G. J. (2013). Tectono-magmatic evolution of the younger Gardar southern rift, South Greenland. *Geological Survey of Denmark and Greenland (Geus) Bulletin* **29**, 1–24.

Upton, B. G. J., Skovgaard, A. C., McClurg, J. E., Kirstein, L., Cheadle, M. J., Emeleus, C. H., Wadsworth, W. J. & Fallick, A. E. (2002). Picritic magmas and the Rum ultramafic complex, Scotland. *Geological Magazine* **139**, 437–452.

van Wyk de Vries, B. & Merle, O. (1998). Extension induced by volcanic loading in regional strike-slip zones. *Geology* **26**, 983–986.

Volker, J. A. (1983). The geology of the Trallval area, Rhum, Inner Hebrides. Ph.D. thesis, University of Edinburgh.

Volker, J. A. & Upton, B. G. J. (1990). The structure and petrogenesis of the Trallval and Ruinsival areas of the Rhum ultrabasic complex. *Transactions of the Royal Society of Edinburgh: Earth Sciences* **81**, 69–88. [10.1017/S0263593300005137]

Wadsworth, W. J. (1961). The Layered Ultrabasic Rocks of South-West Rhum, Inner Herbrides. *Philosophical Transactions of the Royal Society B: Biological Sciences* **244B**, 21–64.

Wadsworth, W. J. (1992). Ultrabasic igneous breccias of the Long Loch area, Isle of Rum. *Scottish Journal of Geology* **28**, 103–113.

Wager, L. R. (1963). The mechanism of adcumulus growth in the layered series of the Skaergaard intrusion. *Mineralogical Society of America Special Paper* **1**, 1–9.

Wager, L. R. & Brown, G. M. (1968). *Layered Igneous Rocks*. Edinburgh: Oliver and Boyd.

Wager, L. R., Brown, G. M. & Wadsworth, W. J. (1960). Types of Igneous Cumulates. *Journal of Petrology* **1**, 73–85.

Wager, L. R. & Deer, W. A. (1939). Geological investigations in East Greenland. Part III. The petrology of the Skaergaard intrusion, Kangerdlussuaq, East Greenland. Copenhagen, Denmark. *Meddelelser om Grønland* **105**, 352.

Walker, G. P. L. (1975). A new concept of the evolution of the British Tertiary intrusive centres. *Journal of the Geological Society* **131**, 121–141.

Weis, F. A., Skogby, H., Troll, V. R., Deegan, F. M. & Dahrén, B. (2015). Magmatic water contents determined through clinopyroxene: Examples from the Western Canary Islands, Spain. *Geochemistry, Geophysics, Geosystems* **16**, 2127–2146.